

Magnetic resonance in quantum computing and in accurate measurements of the nuclear moments of atoms and molecules

Zhichen Liu¹ and Richard A. Klemm^{1, 2, *}

¹Department of Physics, University of Central Florida, Orlando, FL 32816-2385, USA

²U. S. Air Force Research Laboratory, Wright-Patterson Air Force Base, Ohio 45433-7251, USA

(Dated: February 19, 2026)

With modern experimental techniques, it is now possible to generate magnetic fields with the precise form, $\mathbf{H}(t) = H_0\hat{\mathbf{z}} + H_1[\hat{\mathbf{x}} \cos(\omega t) + \hat{\mathbf{y}} \sin(\omega t)]$, both at frequencies within an order of magnitude of the nuclear magnetic resonance (NMR) and of the electron paramagnetic resonance (EPR) frequencies, ω_{n0} and ω_{e0} , respectively, when acting on atoms or molecules. We found simple forms for the exact wave functions of the nuclear and electronic spins that allow for transitions between entangled states, allowing an atom or molecule to function as a quantum computer. These forms also allow for precise NMR or EPR measurements of the nuclear moments in atoms or molecules. Examples relevant to measurements of the nuclear moments of ^{14}N , ^7Li , and ^{133}Cs are given. Since present hyperfine measurements of the lowest three nuclear moments of ^{133}Cs are inconsistent with each other, the proposed NMR or EPR experiments allow one to measure all seven of its nuclear moments with high precision.

I. INTRODUCTION

Nuclear magnetic moments have spin quantum numbers I that for light stable isotopes are $\frac{1}{2}$ for ^1H and ^{13}C , 1 for ^2H and ^{14}N , $\frac{3}{2}$ for ^7Li , ^9Be , and ^{11}B , $\frac{5}{2}$ for ^{17}O , 3 for ^{10}B , and for heavy stable isotopes, it is $\frac{7}{2}$ for ^{133}Cs and up to $\frac{9}{2}$ for ^{83}Kr , ^{87}Sr , ^{93}Nb , ^{113}In , ^{179}Hf , and ^{209}Bi , and to yet higher values for long-lived unstable nuclei [1, 2]. As first shown by Ramsey [3], nuclei with spin I can have $2I$ moments, with the matrix set $\hat{\delta V}_{ne}$ of those nuclear \mathbf{I} and electronic \mathbf{J} spin angular momentum operators given by

$$\hat{\delta V}_{ne} = \sum_{q=0}^{2I} K_q (\mathbf{I} \cdot \mathbf{J} / \hbar^2)^q \mathbf{1}_n \otimes \mathbf{1}_e, \quad (1)$$

where $\mathbf{1}_n$ and $\mathbf{1}_e$ are identity matrices of respective ranks $2I+1$ and $2J+1$, the K_q are real functions of I and J and the components of \mathbf{I} and of \mathbf{J} satisfy independent Lie algebras, each of the form

$$[O_\lambda, O_\mu] = i\hbar\epsilon_{\lambda\mu\nu}O_\nu, \quad (2)$$

where $[I_\lambda, J_\mu] = 0$, $\hbar = \frac{h}{2\pi}$, h is Planck's constant, $\epsilon_{\lambda\mu\nu}$ is the Levi-Civita symbol, and repeated subscripts are implicitly summed over. Eq. (1) implies that nuclei with $I = \frac{1}{2}$ exhibit magnetic dipole moments, those with $I = 1$ have both magnetic dipole and electric quadrupole moments, and those with $I = \frac{3}{2}$ also have magnetic octupole moments, etc. Explicit formulas for the K_q for $0 \leq q \leq 3$ valid for those three moments are available [4, 5]. However, for $I > \frac{3}{2}$, hexadecapole and yet higher moments can exist, and if so, they will contribute to the K_q for $q > 3$ and also to the K_q expressions for $0 \leq q \leq 3$. An

important example discussed in the following is ^{133}Cs , for which present hyperfine measurements of the lowest three of its seven nuclear moments have been at least somewhat inconsistent with one another [6], possibly because all higher moments were assumed to vanish.

Traditionally, such moments have been easiest to measure by careful examinations of the electronic hyperfine structure of an atom [4, 5, 7–9]. In the following, we show that it is possible to make much more accurate measurements of the nuclear moments using either nuclear magnetic resonance (NMR) or electron paramagnetic resonance (EPR) experiments. That is, by appropriate designs of solenoids, magnetic fields can presently be generated to have the rotating wave form (RWF)

$$\mathbf{H}(t) = H_0\hat{\mathbf{z}} + H_1[\hat{\mathbf{x}} \cos(\omega t) + \hat{\mathbf{y}} \sin(\omega t)], \quad (3)$$

over a wide range of angular frequencies ω . With this form, the time-dependent part of the magnetic field rotates about the time-independent field component. Usually one has $H_1/H_0 \ll 1$, and for NMR and EPR experiments, one needs to have ω variable over at least an order of magnitude around the respective resonant values ω_{n0} and ω_{e0} described in the following. More complicated periodic time dependencies described by Fourier series can also be presently generated.

Historically, in early standard magnetic resonance experiments [3, 10–13], the Hamiltonian $\hat{H}(t)$ for the interaction of the nuclear spin \mathbf{I} with the applied magnetic field $\mathbf{H}(t)$ at the time t has a form similar to $\hat{H}(t) = \mu_n \mathbf{I} \cdot [H_0\hat{\mathbf{z}} + H_1\hat{\mathbf{x}} \cos(\omega t)]$, where μ_n is the magnetic moment appropriate for the studied nuclear isotope.

Although the exact solution to this problem has not been published for general I , especially in a form suitable to treat the atomic and molecular interactions of the various nuclear moments with their surrounding electrons, those authors found that one could make great progress by use of magnetic fields of the RWF, in which the oscillatory field component rotates about the constant field

* richard.klemm@ucf.edu, corresponding author

component precisely as in Eq. (3), the bare, or nominally independent nuclear Hamiltonian of which is

$$\hat{H}_n^0(t) = \omega_{n0}I_z + \omega_{n1}[I_x \cos(\omega t) + I_y \sin(\omega t)], \quad (4)$$

where $\omega_{n0} = \mu_n(1 - \sigma)H_0$, $\omega_{n1} = \mu_n(1 - \sigma')H_1$, σ and σ' are the chemical shifts along and normal to \mathbf{z} , and usually $|\omega_{n1}/\omega_{n0}| \ll 1$ [3, 10–16]. We note that the chemical shifts are very weak perturbations, usually measured in parts per million (ppm) due to the particular surrounding electronic environment that has long been used by organic chemists to aid in the identification of the molecular locations of the probed nuclei [17–19].

Early treatments of this problem in terms of $2I$ Pauli matrices by Majorana, Rabi, Ramsey, and Schwinger were correct [3, 10–14], and the derivation for arbitrary $\mathbf{H}(t)$ and I , while complicated, could eventually be found if the exact solution for $I = \frac{1}{2}$ were known [14].

Gottfried removed the t dependence of $\hat{H}(t)$ in Eq. (4) by performing a rotation about the z axis by the t -dependent “angle” $-\omega t$, obtaining for general nuclear spin I [15],

$$|\psi_{G,n}(t)\rangle = e^{-iI_z\omega t/\hbar}e^{-i\hat{H}_{\text{eff},n}t/\hbar}|\psi_{G,n}(0)\rangle, \quad (5)$$

where the basis for $|\psi_{G,n}(0)\rangle$ consists of the complete set of eigenstates $|I, m\rangle$ of \mathbf{I}^2 and I_z ,

$$\begin{aligned} \mathbf{I}^2|I, m\rangle &= \hbar^2 I(I+1)|I, m\rangle, \\ I_z|I, m\rangle &= \hbar m|I, m\rangle, \end{aligned} \quad (6)$$

and

$$\hat{H}_{\text{eff},n} = (\omega_{n0} - \omega)I_z + \omega_{n1}I_x. \quad (7)$$

Gottfried then correctly wrote the nuclear spin wave function $|\psi_{G,n}(t)\rangle$ (in our notation) as

$$|\psi_{G,n}(t)\rangle = e^{-iI_z\omega t/\hbar}e^{-i\hat{\mathbf{n}}_n \cdot \mathbf{I}\Omega_n t/\hbar}|\psi_{G,n}(0)\rangle, \quad (8)$$

where

$$\hat{\mathbf{n}}_n = \hat{\mathbf{z}} \cos(\beta_n) + \hat{\mathbf{x}} \sin(\beta_n), \quad (9)$$

$$\cos(\beta_n) = \frac{\omega_{n0} - \omega}{\Omega_n}; \quad \sin(\beta_n) = \frac{\omega_{n1}}{\Omega_n} \quad (10)$$

and

$$\Omega_n = \sqrt{(\omega_{n0} - \omega)^2 + \omega_{n1}^2}. \quad (11)$$

Gottfried then wrote that for the probability amplitude for a transition from the single nuclear occupied initial state $|\psi_n(0)\rangle = |I, m\rangle$ to the single occupied final state $|I, m'\rangle$ at the time t is given by

$$\langle I, m' | e^{-iI_z\omega t/\hbar}e^{-i\hat{\mathbf{n}}_n \cdot \mathbf{I}\Omega_n t/\hbar} | I, m \rangle = e^{-im'\omega t} d_{m',m}^{(I)}[\tilde{\beta}_n(t)], \quad (12)$$

where

$$\sin\left[\frac{1}{2}\tilde{\beta}_n(t)\right] = \frac{\omega_{n1}}{\Omega_n} \sin\left(\frac{\Omega_n t}{2}\right), \quad (13)$$

and therefore that the probability $P_{m',m}(t)$ of a transition from the initial nuclear single-state $|I, m\rangle$ to the nuclear single-state $|I, m'\rangle$ at the time t is given by

$$P_{m',m}(t) = |d_{m',m}^{(I)}[\tilde{\beta}_n(t)]|^2. \quad (14)$$

Although Eqs. (8) to (14) are correct, as shown in Sec. VI, Eqs. (8) and the non-trivial t dependence of (13) can be rather cumbersome to employ in perturbation treatments of experimentally relevant Hamiltonians. It is also cumbersome to use it to describe transitions between mixed or entangled states in order to make it useful in quantum computing. Since the matrix elements of $d_{m',m}^{(I)}(\beta_n)$ are known when β_n represents the second Euler angle rotation proportional to $\langle I, m' | \exp(-i\beta_n I_y/\hbar) | I, m \rangle$ [16], in which the operator I_y is not present in $H_{\text{eff},n}$, so additional rotations are implicit in Gottfried’s expression for $\tilde{\beta}_n(t)$, Eq. (13). The equivalence of Gottfried’s wave function, Eq. (8), and the present useful exact wave function derived in Sec. II is shown explicitly for $I = 1$ in the Appendix. However, as shown in the following, the present useful exact wave function form is considerably easier to employ in such perturbation expansions. The present form also allows one to calculate the probability of a transition from a fully general state to another fully general state, which can be useful in quantum computing.

In addition, we note that the second exponential factor in $|\psi_{G,n}(t)\rangle$ in Eq. (8) can be written as e^{u+v} where $u = -it \sin(\beta_n) I_x/\hbar$ and $v = -it \cos(\beta_n) I_z/\hbar$, where I_x and I_z satisfy the Lie algebra given by Eq. (2). One could in principle employ the Campbell-Baker-Hausdorff-Dynkin theorem to rewrite this in an infinite series of powers of uv [20]. However, such a power series would not only be an infinite series in powers of $t^2 I_x I_z$, its extreme complexity in form would make expressions for transitions from one general state to another extremely complicated. It would also greatly complicate its use by experimentalists in measurements of physical properties such as nuclear moments.

Here a similar technique to obtain Eqs. (5) and (7) is used [3, 10–15], but an elementary procedure to rewrite the wavefunction in Eq. (8) in terms of products of exponentials of single spin operators valid for arbitrary I and to generalize it to arbitrary J is added [22? , 23]. This allows one to find the useful exact operator form for the general wavefunction $|\psi(t)\rangle$, allowing both the initial state (at $t = 0$) and the state at time t to be the most general linear combinations of the substates, and hence to obtain an exact expression for the most general complete set of eigenstate occupation amplitudes $C_{m'}(t)$ at an arbitrary time $t \geq 0$ based upon their most general complete set of initial occupation amplitudes $C_m(0)$. Some textbooks [16, 24] solved the simplest case $I = \frac{1}{2}$ for one state initially occupied.

In Sec. II, the derivations of the useful exact wave functions for both NMR with arbitrary I and EPR for arbitrary J using magnetic fields of the form in Eq. (3),

a combined form useful for accurate perturbation corrections to that magnetic field form are presented in detail. Both are needed to calculate the nuclear moment energies from Eq. (1). A fully general expression for the electric quadrupole moment energies is derived, and the exact energies for $I = 1, J = \frac{1}{2}$ are found. In Sec. III, the adiabatic approximation is given for general eigenstates. In Sec. IV, the occupation amplitudes and probabilities and the resonance condition are given. In Sec. V, numerical results for $\frac{1}{2} \leq I \leq 2$ under three different initial conditions are presented. In Sec. VI, the uses of the exact combined NMR and EPR wave function to treat a variety of Hamiltonians accurately at and near to resonance conditions are presented. In order to treat the nuclear moment energies, it is necessary to first obtain the analogous useful exact wave function for the electronic angular momentum J states. Our method can in principle solve exactly for the energies of the entire nuclear moment series in Eq. (1), which could be crucial in determining the seven nuclear moments of ^{133}Cs . Finally, in Sec. VII, the summary and conclusions are provided.

II. THE USEFUL EXACT SOLUTION

A. The useful exact nuclear wave function

Starting with $\hat{H}_n^0(t)$ in Eq. (4), one first rotates I_x and I_y by an angle ϕ about the z axis, [15, 16, 24–27]

$$\begin{aligned} I_x(\phi) &= e^{iI_z\phi/\hbar} I_x e^{-iI_z\phi/\hbar}, \\ I_y(\phi) &= e^{iI_z\phi/\hbar} I_y e^{-iI_z\phi/\hbar}. \end{aligned} \quad (15)$$

Taking the derivatives of these equations with respect to ϕ , one may write

$$\begin{aligned} \frac{\partial I_x(\phi)}{\partial \phi} &= \frac{i}{\hbar} e^{iI_z\phi/\hbar} [I_z, I_x] e^{-iI_z\phi/\hbar} = -I_y(\phi), \\ \frac{\partial I_y(\phi)}{\partial \phi} &= \frac{i}{\hbar} e^{iI_z\phi/\hbar} [I_z, I_y] e^{-iI_z\phi/\hbar} = I_x(\phi), \end{aligned} \quad (16)$$

where Eq. (2) was used to evaluate the commutators. By repeating this process, one finds for $i = x, y$,

$$\frac{\partial^2 I_i(\phi)}{\partial \phi^2} + I_i(\phi) = 0, \quad (17)$$

which is the one-dimensional simple harmonic oscillator equation, with solutions $A_i \cos(\phi) + B_i \sin(\phi)$. Imposing the boundary conditions $I_x(0) = I_x$, $I_y(0) = I_y$, and

$$\begin{aligned} \frac{\partial I_x(\phi)}{\partial \phi} \Big|_{\phi=0} &= -I_y, \\ \frac{\partial I_y(\phi)}{\partial \phi} \Big|_{\phi=0} &= I_x, \end{aligned} \quad (18)$$

from Eqs. (16) at $\phi = 0$, one easily obtains

$$\begin{aligned} I_x(\phi) &= I_x \cos(\phi) - I_y \sin(\phi), \\ I_y(\phi) &= I_y \cos(\phi) + I_x \sin(\phi), \end{aligned} \quad (19)$$

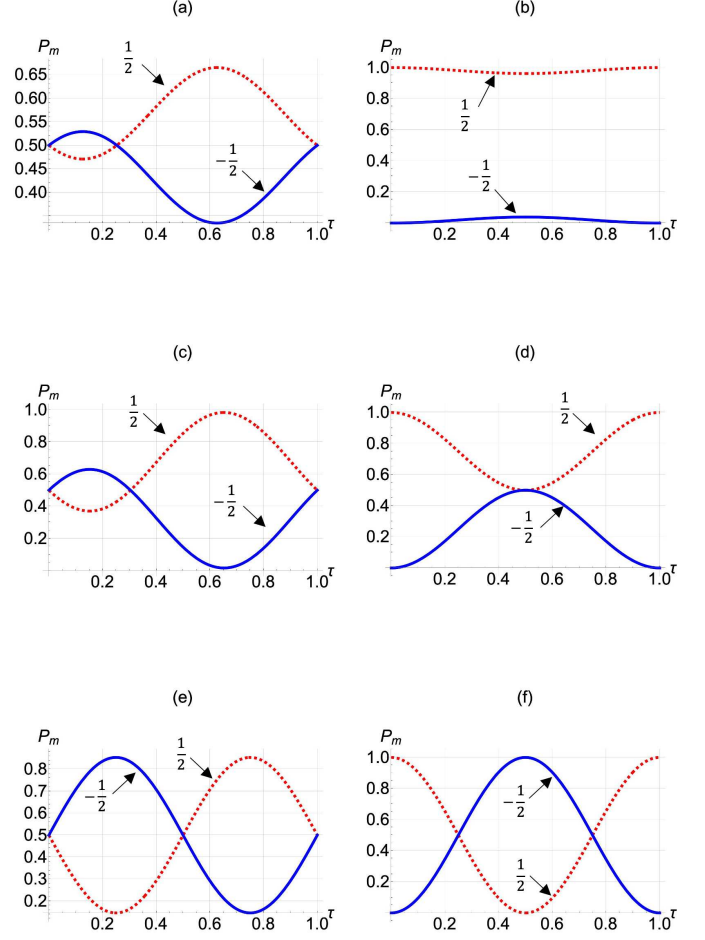


FIG. 1. (Color online) Plots of $P_{1/2}(\tau)$ (dotted red) and $P_{-1/2}(\tau)$ (solid blue) for $I = \frac{1}{2}$ and $0 \leq \tau = t/T_n \leq 1$. In (a), (c), and (e), $C_{1/2}(0)e^{-i\pi/4} = C_{-1/2}(0) = \frac{1}{\sqrt{2}}$. In (b), (d), and (f), $C_{1/2}(0) = 1$ and $C_{-1/2}(0) = 0$. In (a) and (b), $\omega/\omega_{n0} = 0.95$, in (c) and (d), $\omega/\omega_{n0} = 0.99$, and in (e) and (f), $\omega/\omega_{n0} = 1$. This figure also applies for $J = \frac{1}{2}$ with $\tau = t/T_e$ and ω_{n0} and $C_m(0)$ respectively replaced by ω_{e0} and $D_{\bar{m}}(0)$.

as for a classical rotation of the x and y axes by the angle ϕ about the z axis [16]. Letting $\phi \rightarrow -\omega t$ [15], one obtains $I_x(-\omega t)$ given by

$$I_x \cos(\omega t) + I_y \sin(\omega t) = e^{-iI_z\omega t/\hbar} I_x e^{iI_z\omega t/\hbar}. \quad (20)$$

The bare Hamiltonian in Eq. (4) may then be written as

$$\hat{H}_n^0(t) = e^{-iI_z\omega t/\hbar} (\omega_{n0} I_z + \omega_{n1} I_x) e^{iI_z\omega t/\hbar}. \quad (21)$$

One may then solve the Schrödinger equation,

$$\hat{H}_n^0(t) |\psi_n^0(t)\rangle = i\hbar \frac{\partial |\psi_n^0(t)\rangle}{\partial t} \quad (22)$$

by writing

$$|\psi_n^0(t)\rangle = e^{-iI_z\omega t/\hbar}|\psi_n^{0'}(t)\rangle, \quad (23)$$

$$i\hbar \frac{\partial|\psi_n^0\rangle}{\partial t} = \omega I_z e^{-iI_z\omega t/\hbar}|\psi_n^{0'}\rangle + i\hbar e^{-iI_z\omega t/\hbar} \frac{\partial|\psi_n^{0'}\rangle}{\partial t},$$

leading to

$$e^{-iI_z\omega t/\hbar} \left(\omega_{n0} I_z + \omega_{n1} I_x \right) |\psi_n^{0'}\rangle = e^{-iI_z\omega t/\hbar} \left(\omega I_z |\psi_n^{0'}\rangle + i\hbar \frac{\partial|\psi_n^{0'}\rangle}{\partial t} \right), \quad (24)$$

or

$$\hat{H}_{\text{eff},n} |\psi_n^{0'}\rangle = \left[(\omega_{n0} - \omega) I_z + \omega_{n1} I_x \right] |\psi_n^{0'}\rangle = i\hbar \frac{\partial|\psi_n^{0'}\rangle}{\partial t}, \quad (25)$$

where to obtain Eq. (25), both sides of Eq. (24) were multiplied by $\exp(iI_z\omega t/\hbar)$ on the left, and where $\hat{H}_{\text{eff},n}$ is independent of t . Solving Eq. (25) for $|\psi_n'(t)\rangle$, one easily finds

$$|\psi_n^{0'}(t)\rangle = e^{-i\hat{H}_{\text{eff},n}t/\hbar}|\psi_n^{0'}(0)\rangle. \quad (26)$$

Combining Eqs. (26) and (23) with the initial conditions $|\psi_n^{0'}(0)\rangle = |\psi_n^0(0)\rangle$, one obtains Gottfried's Eq. (5) [15].

As Gottfried correctly argued, $\hat{H}_{\text{eff},n}$ can be diagonalized by rotating \mathbf{I} about the y axis by an angle β_n so that $\mathbf{I}(\beta_n)||\hat{z}$. In order to determine how the wave function changes, it is useful to diagonalize the second exponential operator factor in the wave function given by Eq. (5), which Gottfried did not do. By inserting $\mathbf{1}_n = e^{-i\beta_n I_y/\hbar} e^{i\beta_n I_y/\hbar}$ between and to the right of the two exponential operators in Eq. (5), where $\mathbf{1}_n$ is the identity matrix of rank $2I+1$, one finds that

$$|\psi_n^0(t)\rangle = e^{-iI_z\omega t/\hbar} e^{-i\beta_n I_y/\hbar} \mathcal{O}(\beta_n, t) e^{+i\beta_n I_y/\hbar} \times |\psi_n^0(0)\rangle, \quad (27)$$

where

$$\mathcal{O}(\beta_n, t) = e^{+i\beta_n I_y/\hbar} e^{-i\hat{H}_{\text{eff},n}t/\hbar} e^{-i\beta_n I_y/\hbar}. \quad (28)$$

By defining

$$\hat{H}_{\text{eff},n}(\beta_n) = e^{+i\beta_n I_y/\hbar} \hat{H}_{\text{eff},n} e^{-i\beta_n I_y/\hbar}, \quad (29)$$

one may then evaluate $\mathcal{O}(\beta_n, t)$ by expanding $e^{-i\hat{H}_{\text{eff},n}t/\hbar}$ in Eq. (28) in a power series in $\hat{H}_{\text{eff},n}$, inserting $\mathbf{1}_n = e^{-i\beta_n I_y/\hbar} e^{i\beta_n I_y/\hbar}$ between each pair of $\hat{H}_{\text{eff},n}$ operators, transforming each $\hat{H}_{\text{eff},n}$ to $\hat{H}_{\text{eff},n}(\beta_n)$ by Eq. (29), and resumming the series, leading to

$$\mathcal{O}(\beta_n, t) = e^{-i\hat{H}_{\text{eff},n}(\beta_n)t/\hbar}. \quad (30)$$

Using the same procedure as in Eqs. (15)-(19), the rotated $I_x(\beta_n)$ and $I_z(\beta_n)$ in Eq. (29) are

$$I_x(\beta_n) = I_x \cos(\beta_n) + I_z \sin(\beta_n), \quad (31)$$

$$I_z(\beta_n) = I_z \cos(\beta_n) - I_x \sin(\beta_n), \quad (32)$$

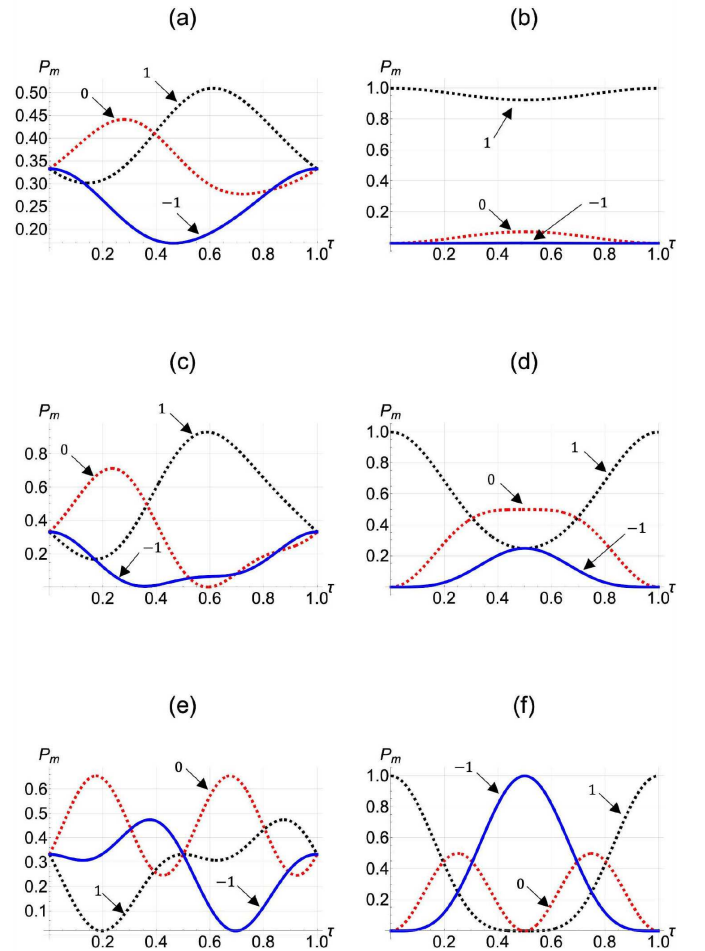


FIG. 2. (Color online) Plots of $P_1(\tau)$ (dotted black), $P_0(\tau)$ (dotted red) and $P_{-1}(\tau)$ (solid blue) for $I = 1$ and $0 \leq \tau = t/T_n \leq 1$. In (a), (c), and (e), $C_0(0) = C_{-1}(0) = e^{-i\pi/4}C_1(0) = \frac{1}{\sqrt{3}}$. In (b), (d), and (f), $C_1(0) = 1$ and $C_0(0) = C_{-1}(0) = 0$. In (a) and (b), $\omega/\omega_{n0} = 0.95$, in (c) and (d), $\omega/\omega_{n0} = 0.99$, and in (e) and (f), $\omega/\omega_{n0} = 1$. This figure also applies for $J = 1$ with $\tau = t/T_e$ and ω_{n0} and $C_m(0)$ respectively replaced by ω_{e0} and $D_{\bar{m}}(0)$.

so that

$$\hat{H}_{\text{eff},n}(\beta_n) = (\omega_{n0} - \omega)[I_z \cos(\beta_n) - I_x \sin(\beta_n)] + \omega_{n1}[I_x \cos(\beta_n) + I_z \sin(\beta_n)]. \quad (33)$$

Equations (10) force the off-diagonal terms to vanish, leading to

$$\hat{H}_{\text{eff},n}(\beta_n) = \Omega_n I_z, \quad (34)$$

where Ω_n is given by Eq. (11). Then from Eqs. (27), (30), and (34), one finds

$$|\psi_n^0(t)\rangle = e^{-iI_z\omega t/\hbar} e^{-i\beta_n I_y/\hbar} e^{-iI_z\Omega_n t/\hbar} e^{i\beta_n I_y/\hbar} |\psi_n^0(0)\rangle, \quad (35)$$

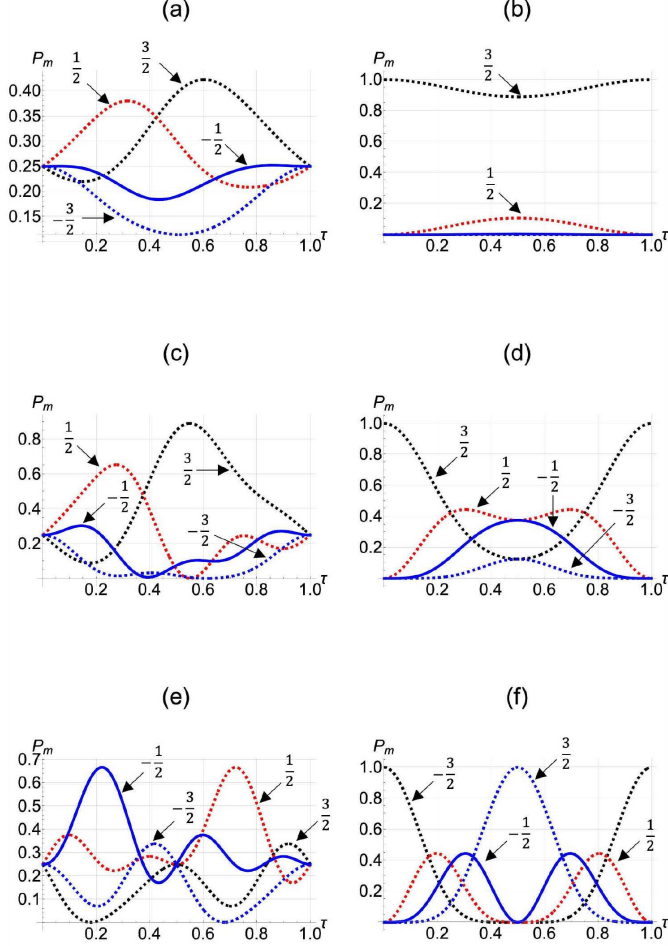


FIG. 3. (Color online) Plots of $P_{3/2}(\tau)$ (dotted black), $P_{1/2}(\tau)$ (dotted red), $P_{-1/2}(\tau)$ (solid blue), and $P_{-3/2}(\tau)$ (dotted blue) for $I = \frac{3}{2}$ and $0 \leq \tau = t/T_n \leq 1$. In (a), (c), and (e), $C_{-\frac{3}{2}}(0) = C_{-\frac{1}{2}}(0) = C_{\frac{1}{2}}(0) = e^{-i\pi/4}C_{\frac{3}{2}}(0) = \frac{1}{2}$. In (b), (d), and (f), $C_{\frac{3}{2}}(0) = 1$ and $C_m(0) = 0$ for $m \neq \frac{3}{2}$. In (a) and (b), $\omega/\omega_{n0} = 0.95$, in (c) and (d), $\omega/\omega_{n0} = 0.99$, and in (e) and (f), $\omega/\omega_{n0} = 1$. This figure also applies for $J = \frac{3}{2}$ with $\tau = t/T_e$ and m, ω_{n0} and $C_m(0)$ respectively replaced by \bar{m}, ω_{e0} , and $D_{\bar{m}}(0)$.

which is also an exact but a more useful operator form of $|\psi_n(t)\rangle$, where β_n and Ω_n are respectively given by Eqs. (10) and (11). It is straightforward to prove that $|\psi_n(t)\rangle$ given by Eq. (35) exactly satisfies the Schrödinger wave equation,

$$i\hbar \frac{\partial}{\partial t} |\psi_n^0(t)\rangle = \hat{H}_n^0(t) |\psi_n^0(t)\rangle, \quad (36)$$

where $\hat{H}_n^0(t)$ is given by Eqs. (4). As discussed in Sec. IV, we choose to define $\beta_n = \sin^{-1}(\omega_{n1}/\Omega_n)$, which is an even function of $\omega - \omega_{n0}$ that is independent of t .

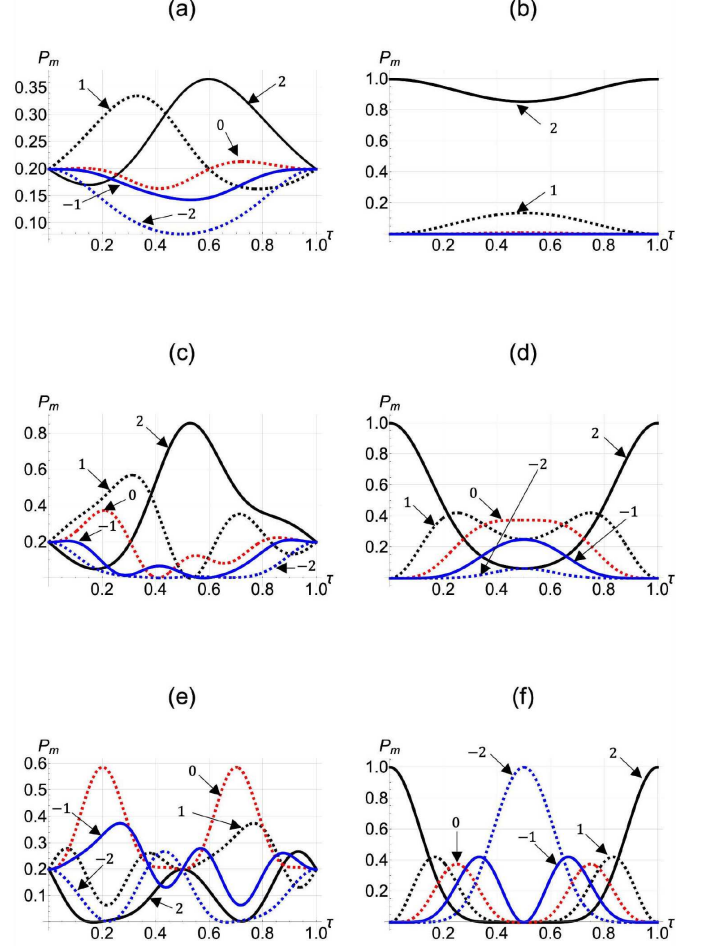


FIG. 4. (Color online) Plots of $P_2(\tau)$ (solid black), $P_1(\tau)$ (dotted black), $P_0(\tau)$ (dotted red), $P_{-1}(\tau)$ (solid blue), and $P_{-2}(\tau)$ (dotted blue) for $I = 2$ and $0 \leq \tau = t/T_n \leq 1$. In (a), (c), and (e), $C_{-2}(0) = C_{-1}(0) = C_0(0) = C_1(0) = e^{-i\pi/4}C_2(0) = \frac{1}{\sqrt{5}}$. In (b), (d), and (f), $C_2(0) = 1$ and $C_m(0) = 0$ for $m \neq 2$. In (a) and (b), $\omega/\omega_{n0} = 0.95$, in (c) and (d), $\omega/\omega_{n0} = 0.99$, and in (e) and (f), $\omega/\omega_{n0} = 1$. This figure also applies for $J = 2$ with $\tau = t/T_e$ and m, ω_{n0} , and $C_m(0)$ respectively replaced by \bar{m}, ω_{e0} , and $D_{\bar{m}}(0)$.

Then by writing

$$|\psi_n^0(t)\rangle = \sum_{m'=-I}^I C_{m'}(t) |I, m'\rangle, \quad (37)$$

taking the inner product $\langle I, m | \psi_n^0(t) \rangle$ and using Eqs. (35) and (37), the latter both at $t = 0$ and at $t > 0$, one obtains

$$C_m(t) = \sum_{m'=-I}^I C_{m'}(0) \langle I, m | e^{-iI_z\omega t/\hbar} e^{-iI_y\beta_n/\hbar} e^{-iI_z\Omega_n t/\hbar} \times e^{iI_y\beta_n/\hbar} | I, m' \rangle, \quad (38)$$

where eigenstate orthonormality

$$\langle I, m | I, m' \rangle = \delta_{m,m'} \quad (39)$$

was employed. After introducing identity operators such as

$$\sum_{m''=-I}^I |I, m''\rangle \langle I, m''| = \mathbf{1}_n \quad (40)$$

between each of the exponential operators in Eq. (38), and making use of Eqs. (6) and (39), one finds

$$\begin{aligned} C_m(t) &= \sum_{m', m'', m''', m''''=-I}^I C_{m'}(0) \langle I, m | e^{-iI_z\omega t/\hbar} | I, m'' \rangle \\ &\quad \times \langle I, m'' | e^{-i\beta_n I_y/\hbar} | I, m'' \rangle \\ &\quad \times \langle I, m'' | e^{-iI_z\Omega_n t/\hbar} | I, m'''' \rangle \langle I, m'''' | e^{i\beta_n I_y/\hbar} | I, m' \rangle \\ &= e^{-im\omega t} \sum_{m', m''=-I}^I C_{m'}(0) e^{-im''\Omega_n t} \\ &\quad \times \langle I, m | e^{-i\beta_n I_y/\hbar} | I, m'' \rangle \langle I, m'' | e^{i\beta_n I_y/\hbar} | I, m' \rangle \\ &= e^{-im\omega t} \sum_{m', m''=-I}^I C_{m'}(0) e^{-im''\Omega_n t} \\ &\quad \times d_{m', m''}^{(I)}(\beta_n) d_{m', m''}^{(I)*}(\beta_n), \end{aligned} \quad (41)$$

where $d_{m', m}^{(I)}(\beta_n)$ is the reduced rotation matrix element for the second Euler angle, as derived by Wigner and detailed in textbooks [15, 16, 27],

$$\begin{aligned} d_{m', m}^{(I)}(\beta_n) &\equiv \langle I, m' | e^{-i\beta_n I_y/\hbar} | I, m \rangle \\ &= \sum_k (-1)^{k-m+m'} \\ &\quad \times \frac{\sqrt{(I+m)!(I-m)!(I+m')!(I-m')!}}{(I+m-k)!k!(I-k-m')!(k-m+m')!} \\ &\quad \times \left[\cos(\beta_n/2) \right]^{2I-2k+m-m'} \\ &\quad \times \left[\sin(\beta_n/2) \right]^{2k-m+m'}, \end{aligned} \quad (42)$$

where k takes on all values for which none of the arguments of the factorials in the denominator are negative [16]. That is, $\max(0, m - m') \leq k \leq \min(I + m, I - m')$. In Eq. (42),

$$\sin(\beta_n/2) = \sqrt{\frac{1 - \cos(\beta_n)}{2}} = \sqrt{\frac{\Omega_n + \omega - \omega_{n0}}{2\Omega_n}}, \quad (43)$$

$$\cos(\beta_n/2) = \sqrt{\frac{1 + \cos(\beta_n)}{2}} = \sqrt{\frac{\Omega_n + \omega_{n0} - \omega}{2\Omega_n}}, \quad (44)$$

which are both finite and independent of t for any ω .

The t dependence of Eq. (41) has the same form as that of Hall and Klemm [28], who showed it to be valid for

$I = \frac{1}{2}, 1, \frac{3}{2}$, but did not evaluate the constant coefficients. That $T = 0$ model was subsequently extended to finite T [29].

Many workers have used the Gottfried wave function for general I or Pauli matrices for $I = \frac{1}{2}$ to treat general I NMR and N -level quantum systems exhibiting SU(2) symmetry [30–44]. Some of those workers used the Gottfried wave function to evaluate the probability of a transition from a single fully-occupied state to another single fully-occupied state, and their figures appear to be identical to ours, even for $I = \frac{9}{2}$ (or $N = 10$), as were presented elsewhere [23]. In some cases they did it purely by numerical techniques, and in some other cases they used Gottfried's wave function, and in yet some additional cases, they solved large matrices analytically, but did not write down the wave function. But none of them either wrote Eq. (35) or evaluated analytically the transitions involving two or more initial or final populated states, which is essential in quantum computing.

B. The useful exact bare electronic wave function

In an NMR experiment, the electrons in an atom or molecule surrounding a nucleus are subject to the same time-dependent applied magnetic field as are the nuclei. Correspondingly, the nuclei in an atom or molecule in an EPR experiment are subject to the same time-dependent applied magnetic field as are the electrons. In the absence of interactions between the nuclei and the surrounding electrons, the relevant electronic bare Hamiltonian is

$$\hat{H}_e^0(t) = \omega_{e0} J_z + \omega_{e1} [J_x \cos(\omega t) + J_y \sin(\omega t)], \quad (45)$$

where the total electronic angular momentum operator components J_i also satisfy the standard Lie algebra in Eq. (2), and are independent of the nuclear spin operators I_j , but the quantities $\omega_{e0} = \mu_e H_0$ and $\omega_{e1} = \mu_e H_1$ in Eq. (45), where

$$\mu_e = \frac{ge}{2m_e}, \quad (46)$$

where $m_e = 9.1093837015(28) \times 10^{-31}$ kg [45] and e are the mass and charge of an electron, and where $(g - 2)/2 = \frac{\alpha}{2\pi} + \dots$ [46] includes the complete series of quantum electrodynamics (QED) corrections to the magnetic moment of the electron, and where α is the fine structure constant. To date, to accuracy $(\frac{\alpha}{2\pi})^5$, $(g - 2)/2 = 1159652181.606(11)(12)(229) \times 10^{-12}$, where the three uncertainties in parentheses are respectively from the 10th order QED calculations, the hadron, and the best measurement of the fine structure constant. [47] Since $m_p/m_e = 1836.152673346(81)$ [48], recently improved upon by about a factor of 2 in accuracy, [45], depending upon the particular atom under study, m_e is at least three to five or more orders of magnitude smaller than the mass of the nucleus under study, so that ω_{e0} and

ω_{e1} are three to five orders of magnitude larger than and usually opposite in sign to the analogous nuclear quantities ω_{n0} and ω_{n1} . The magnetic field strengths at the positions of the electrons and the nuclei are assumed to be the same, but the magnetic moments are enormously different, primarily due to the enormously different electronic and nuclear masses.

Then, we may immediately write down the exact bare electronic wave function for an applied magnetic field of the form of Eq. (3),

$$|\psi_e^0(t)\rangle = e^{-iJ_z\omega t/\hbar} e^{-i\beta_e J_y/\hbar} e^{-i\Omega_e J_z t/\hbar} e^{i\beta_e J_y/\hbar} |\psi_e^0(0)\rangle, \quad (47)$$

where

$$\sin(\beta_e) = \frac{\omega_{e1}}{\Omega_e}, \quad \cos(\beta_e) = \frac{\omega_{e0} - \omega}{\Omega_e}, \quad (48)$$

$$\Omega_e = \sqrt{(\omega - \omega_{e0})^2 + \omega_{e1}^2}. \quad (49)$$

We note that when $\omega \approx \omega_{n0}$ for nuclear magnetic resonance studies, the applied frequency ω is three to five orders of magnitude below the electron paramagnetic resonance frequency ω_{e0} , depending upon the particular nuclear mass under study. Correspondingly, in an electron paramagnetic resonance experiment, $\omega \approx \omega_{e0}$, ω is three to five orders of magnitude larger than ω_{n0} . As for the nuclear β_n , we define

$$\beta_e = \sin^{-1}\left(\frac{\omega_{e1}}{\Omega_e}\right). \quad (50)$$

The bare wave function for the start of the perturbation calculation is

$$|\psi_{ne}^0(t)\rangle = |\psi_n^0(t)\rangle \otimes |\psi_e^0(t)\rangle, \quad (51)$$

where $|\psi_n^0(t)\rangle$, $|\psi_e^0(t)\rangle$, Ω_n , and Ω_e are respectively given by Eqs. (35), (47), (11), and (49). Although the I_i and J_i operators operate on orthogonal subspaces, one can formally combine $|\psi_n^0(t)\rangle \otimes |\psi_e^0(t)\rangle$ by successively commuting the J_i operators in $|\psi_e^0(t)\rangle$ to the left, maintaining their respective order. We then may write the full atomic wave function as

$$|\psi_{ne}^0(t)\rangle = e^{-i\omega t(I_z \mathbf{1}_e + \mathbf{1}_n J_z)/\hbar} e^{-i(\beta_n I_y \mathbf{1}_e + \beta_e \mathbf{1}_n J_y)/\hbar} \times e^{-it(\Omega_n I_z \mathbf{1}_e + \Omega_e \mathbf{1}_n J_z)/\hbar} \times e^{+i(\beta_n I_y \mathbf{1}_e + \beta_e \mathbf{1}_n J_y)/\hbar} |\psi_{ne}^0(0)\rangle, \quad (52)$$

where $\mathbf{1}_e$ and $\mathbf{1}_n$ are unit matrices of respective ranks $2J+1$ and $2I+1$,

$$|\psi_{ne}^0(0)\rangle = \sum_{m=-I}^I C_m(0) |I, m\rangle \otimes \sum_{\bar{m}=-J}^J D_{\bar{m}}(0) |J, \bar{m}\rangle, \quad (53)$$

and

$$\sum_{\bar{m}=-J}^J |D_{\bar{m}}(0)|^2 = \sum_{m=-I}^I |C_m(0)|^2 = 1 \quad (54)$$

to insure normalization.

III. ADIABATIC APPROXIMATION

In the adiabatic approximation [16, 24, 27, 49], there are no transitions from one state to another, so that

$$C_m^{\text{ad}}(t) = C_m(0) e^{-im\omega t} e^{-im\Omega_n t} |d_{m,m}^{(I)}(\beta_n)|^2, \quad (55)$$

and

$$D_{\bar{m}}^{\text{ad}}(t) = D_{\bar{m}}(0) e^{-i\bar{m}\omega t} e^{-i\bar{m}\Omega_e t} |d_{\bar{m},\bar{m}}^{(I)}(\beta_e)|^2, \quad (56)$$

which can be rewritten as [16, 24, 27, 49]

$$C_m^{\text{ad}}(t) = e^{i\theta_m(t)} e^{i\gamma_m(t)} C_m^{\text{ad}}(0), \quad (57)$$

and

$$D_{\bar{m}}^{\text{ad}}(t) = e^{i\theta_{\bar{m}}(t)} e^{i\gamma_{\bar{m}}(t)} D_{\bar{m}}^{\text{ad}}(0). \quad (58)$$

To identify the dynamic $\theta_m(t), \theta_{\bar{m}}(t)$ and geometric (or Berry) $\gamma_m(t), \gamma_{\bar{m}}(t)$ phase, it is useful to redefine Eqs. (4) and (11) by setting $\omega_n \rightarrow \omega_{n0} \cos \alpha_n$, $\omega_{n1} \rightarrow \omega_{n0} \sin \alpha_n$, $\omega_e \rightarrow \omega_{e0} \cos \alpha_e$, $\omega_{e1} \rightarrow \omega_{e0} \sin \alpha_e$, so that $\mathbf{H}(t)$ “sweeps” along the circular paths at the small angles α_n, α_e about the z axis from the origin to the surface of a sphere [24]. $\theta_m(t) = -m\omega_{n0}t$ and $\theta_{\bar{m}}(t) = -\bar{m}\omega_{e0}t$ are found by time-integrating $-E_m/\hbar = -m\omega_{n0}$ and $-E_{\bar{m}}/\hbar = -\bar{m}\omega_{e0}$, where $E_m, E_{\bar{m}}$ are the energies of the $m^{\text{th}}, \bar{m}^{\text{th}}$ states obtained from Eq. (4) with the present settings for $\omega_{n0}, \omega_{n1}, \omega_{e0}$, and ω_{e1} in the $\omega \rightarrow 0$ limit [16, 24, 27, 49], and $\gamma_m(t), \gamma_{\bar{m}}(t)$ are obtained from Eqs. (55), (57) and the above expressions for $\theta_m(t), \theta_{\bar{m}}(t)$ in the low ω limit far from either resonance, $\omega \ll \omega_{n0}, \omega_{e0}$. [49]. The geometric phases $\gamma_m(T_0)$ and $\gamma_{\bar{m}}(T_0)$ at $t = T_0 = 2\pi/\omega$, the long period of the very slow sweeping motion, equal to the time to complete a closed geometrical orbit, are

$$\begin{aligned} \gamma_m(T_0) &= -m(\omega + \Omega_n)T_0 - \theta_m(T_0) \\ &\approx 2\pi m(\cos \alpha_n - 1), \end{aligned} \quad (59)$$

and

$$\begin{aligned} \gamma_{\bar{m}}(T_0) &= -\bar{m}(\omega + \Omega_e)T_0 - \theta_{\bar{m}}(T_0) \\ &\approx 2\pi \bar{m}(\cos \alpha_e - 1), \end{aligned} \quad (60)$$

which apply for any $-I \leq m \leq I$ and $-J \leq \bar{m} \leq J$, and agrees with the standard result for $I, J = \frac{1}{2}$ [16, 24, 27, 49] and with the result for general $-I \leq m \leq I$ and $-J \leq \bar{m} \leq J$ [27]. Note that for $m = 0$, $\theta_0(t) = \gamma_0(T_0) = 0$.

IV. OCCUPATION PROBABILITIES AND RESONANCE

A. Nuclear spins

By interchanging m and m' in Eq. (38),

$$1 = \langle \psi_n(t) | \psi_n(t) \rangle = \sum_{m'=-I}^I P_{m'}(t), \quad (61)$$

where

$$\begin{aligned} P_{m'}(t) &= |C_{m'}(t)|^2 \\ &= \left| \sum_{m'', m''' = -I}^I C_{m'''}(0) e^{-im''\Omega_n t} \right. \\ &\quad \left. \times d_{m', m''}^{(I)}(\beta_n) d_{m''', m''}^{(I)*}(\beta_n) \right|^2, \end{aligned} \quad (62)$$

is the probability of the occupation of eigenstate $|I, m'\rangle$ at the time t . The sums in Eq. (62) are restricted by $-I \leq m'', m''' \leq I$. Explicitly, $m'', m''' = -I, -I + 1, -I + 2, \dots, I - 2, I - 1, I$, so for integral I , m'', m''' can be any of the integers from $-I$ to I in the sums, and for half-integral I , they can be any of the half-integral values from $-I$ to I in those sums. In order to compare with Gottfried's result, in the special case in which only the $|I, m\rangle$ state is initially occupied,

$$C_{m'''}(0) = \delta_{m, m'''}, \quad (63)$$

then

$$P_{m'}(t) = \left| \sum_{m'' = -I}^I e^{-im''\Omega_n t} d_{m', m''}^{(I)}(\beta_n) d_{m''', m''}^{(I)*}(\beta_n) \right|^2, \quad (64)$$

which for $I > \frac{1}{2}$ has a qualitatively different mathematical form from Gottfried's also correct result. In the above form, there are four d matrices, the argument β_n of each is exactly the time-independent, standard second Euler rotation angle, and the overall t dependence arises only from the elementary exponentials, so that $P_{m'}(t)$ is obviously a periodic function of t nominally with period

$$T_n = \frac{2\pi}{\Omega_n}. \quad (65)$$

The t dependence of this result is consistent with those obtained for $I = \frac{1}{2}, 1, \frac{3}{2}$ by Hall and Klemm [28], although those authors did not provide the details of the time-independent coefficients. For $I = \frac{1}{2}$, this result is also consistent with that of Gottfried [15], who obtained the correct result for $I = \frac{1}{2}$ using the Pauli matrix algebra that is much simpler than that of the Lie algebra required for $I \geq 1$, and wrote the equivalent result in terms of Eqs. (8), (12), and (13). Note that in the above expression, the t dependence of $P_{m'}(t)$ arises from the summation over the m'' state indices that for $I > \frac{1}{2}$ can be different from both the initial m and the final m' state indices. In Gottfried's result with only two d matrix factors, the t dependence is implicitly given by Eq. (13).

Resonance occurs for general I when $\omega = \omega_{n0}$, for which $\beta_n = \frac{\pi}{2}$ in Eqs. (43) and (44) and the $d_{m', m}^{(I)}(\frac{\pi}{2})$ in Eq. (42) are independent of ω, ω_{n0} , and ω_{n1} .

$|\psi_{RW, n}(t)\rangle$ in Eq. (35) and $C_m(t)$ in Eq. (41) have overall phase factors proportional to ω that are different for $\omega = \omega_0 \pm \delta\omega$. However, by defining $\beta_n = \sin^{-1}(\omega_{n1}/\Omega_n)$ from the left expression in Eq. (10),

and since Ω_n given by Eq. (11), β_n is an even function of $\omega - \omega_{n0}$ and $P_m(t)$ is also an even function of $\omega - \omega_{n0}$, which were verified numerically using Eqs. (42) to (44). It has been well established that for $I = \frac{1}{2}$, the resonance curves of $P_{\pm\frac{1}{2}}(t)$ have Lorentzian forms [15, 16, 24, 27]. However, for general I values, especially for integral I , the consequences of resonance depend more strongly upon the initial conditions than they do for the $I = \frac{1}{2}$ case presented in existing textbooks [15, 16, 24, 27].

B. Electronic total angular momentum states

The probability of occupation of the $-J \leq \bar{m}' \leq J$ electronic state is exactly analogous to that of the m' nuclear state in the previous subsection, except that I is replaced by J , and β_n, Ω_n , and T_n are respectively replaced by β_e, Ω_e , and $T_e = 2\pi/\Omega_e$. For example, we have

$$\begin{aligned} P_{\bar{m}'}(t) &= |D_{\bar{m}'}(t)|^2 \\ &= \left| \sum_{\bar{m}'', \bar{m}''' = -J}^J D_{\bar{m}'''}(0) e^{-i\bar{m}''\Omega_e t} \right. \\ &\quad \left. \times d_{\bar{m}', \bar{m}''}^{(I)}(\beta_e) d_{\bar{m}''', \bar{m}''}^{(I)*}(\beta_e) \right|^2. \end{aligned} \quad (66)$$

V. NUMERICAL RESULTS FOR $\frac{1}{2} \leq I, J \leq 2$

A. Time-dependent occupation probability functions

To present some of the more interesting features of magnetic resonance for general I or J , the experimentally relevant ratios $\omega_{n1}/\omega_{n0} = 0.01$ and $\omega_{e1}/\omega_{e0} = 0.01$ in Figs. 1 - 4 were chosen. In Figs. 1 - 4, plots of $P_m(\tau)$ for either $0 \leq \tau = t/T_n \leq 1$ or $0 \leq \tau = t/T_e \leq 1$, where T_n is given by Eq. (65) and $T_e = 2\pi/\Omega_e$, and the m, \bar{m} substates for all I, J values from $\frac{1}{2}$ to 2 with two different initial conditions are presented. In each of these figures, the top, middle, and bottom figure pairs are for ω/ω_{n0} or $\omega/\omega_{e0} = 0.95, 0.99$, and 1, which are respectively in the tail, at the half maximum, and at resonance, or the maximum of the assumed Lorentzian lineshapes. The results for ω/ω_{n0} or $\omega/\omega_{e0} = 0.95, 0.99$ were also obtained respectively for ω/ω_{n0} or $\omega/\omega_{e0} = 1.05, 1.01$. In each row, the left figures assume that all $P_m(0)$ are equal, but respectively $C_I(0)$ and $D_J(0)$ have phase differences of $\pi/4$ from all of the other $C_m(0)$ or $D_{\bar{m}}(0)$ values, and the right figures are for $C_I(0) = 1$ or $D_J(0) = 1$ and the other $C_m(0) = 0$ or $D_{\bar{m}}(0) = 0$. In each of figures (b), (d), and (f), the $P_m(\tau)$ or $P_{\bar{m}}(\tau)$ curves all exhibit even reflection symmetry about $\tau = \frac{1}{2}$, but in (a), (c), and (e), the $P_m(\tau)$ or $P_{\bar{m}}(\tau)$ curves have no such symmetry, although at resonance, the $P_m(\tau)$ or $P_{\bar{m}}(\tau)$ curves in each (e) figure are all equal at $\tau = 0, \frac{1}{2}, 1$, and the $P_m(\tau)$ and $P_{-m}(\tau)$ or $P_{\bar{m}}(\tau)$ and $P_{-\bar{m}}(\tau)$ curves in each (e) and (f)

figure are identical but out of phase by $T_n/2$ or $T_e/2$. For integral I and $m = 0$ or integral J and $\bar{m} = 0$, the resonant period of $P_0(\tau)$ abruptly changes to $T_n/2$ or $T_e/2$ for both initial conditions shown. Analogous cases for $\frac{5}{2} \leq I, J \leq \frac{9}{2}$ are shown elsewhere [23].

The simplest cases for $I = \frac{1}{2}$ or $J = \frac{1}{2}$ are shown in Fig. 1. For the equal initial probability condition, Figs. 1(a) and 1(c) show that the maximal values of $P_{\frac{1}{2}}(\tau)$ are larger than those of $P_{-\frac{1}{2}}(\tau)$. But at resonance, this changes dramatically. Figure 1(e) shows that the $P_{\pm\frac{1}{2}}(\tau)$ curves are identical, except for a phase difference of $T_n/2$ or $T_e/2$. In addition, the periodicity of their points of equal probability is also $T_n/2$ or $T_e/2$. However, for the second initial condition $C_{\frac{1}{2}}(0) = 1$ or $D_{\frac{1}{2}}(0) = 1$, Figs. 1(b) and 1(d) show that as resonance is approached, the maximal values of $P_{-\frac{1}{2}}(\tau)$ increase, but are respectively smaller than the maximal values of $P_{\frac{1}{2}}(\tau)$. However, at resonance, Fig. 1(f) shows that the $P_{\pm\frac{1}{2}}(\tau)$ are equivalent to each other, identically varying from 0 to 1, except for a phase difference of $T_n/2$ or $T_e/2$. Although this problem has been solved in textbooks, the authors all assumed one of the $C_{\pm\frac{1}{2}}(0) = 0$ or $D_{\pm\frac{1}{2}}(0) = 0$, as in Figs. 1(b), 1(d), and 1(f), so the infinite phase difference degeneracy, one example of which is displayed in Figs. 1(a), 1(c), and 1(e), could be ignored [15, 16, 24, 27].

The $P_m(\tau)$ curves for $I = 1$ are shown in Fig. 2. In Figs. 2(a) and 2(c), it can be seen that when all the $P_m(0)$ are equal, but $C_1(0)$ has a phase shift from the other $C_m(0)$, the $P_m(\tau) < 1$ curves are all different, except at $\tau = 0, 1$. In comparing Figs. 2(a) and 2(c), it is evident that for the particular $P_m(0)$ case, the maximal values of $P_m(\tau)$ decrease monotonically with m , just as for $I = \frac{1}{2}$, as shown in Fig. 1. However, this changes dramatically at resonance. In Fig. 2(e), $P_0(\tau)$ has the largest maximum value, the $P_{\pm 1}(\tau)$ are equivalent but out of phase by $T_n/2$ with each other, and the periodicity of the points of equality of all three states is also $T_n/2$. For the other initial condition, $C_1(0) = 1$, by comparing Figs. 2(b) and 2(d), as resonance is approached, the $P_m(\tau)$ for the initially unoccupied states grow, but the maximal values of the $P_m(\tau)$ continue to decrease monotonically with m . But then at resonance, Fig. 2(f) shows that the period of $P_0(\tau)$ changes abruptly from T_n to $T_n/2$. In Fig. 2(f), the equivalent $P_{\pm 1}(\tau)$ alternate between 0 and 1, and are out of phase by $T_n/2$ with each other, and the maximal value of $P_0(\tau)$ is $\frac{1}{2}$. This figure also applies for $J = 1$ with m , $P_m(\tau)$, $C_m(0)$ and T_n respectively replaced by \bar{m} , $P_{\bar{m}}(\tau)$, $D_{\bar{m}}(0)$, and T_e .

In Fig. 3, the analogous $P_m(\tau)$ curves are shown for $I = \frac{3}{2}$. For the equal probability case with $C_{\frac{3}{2}}(0)$ having a phase shift from the other $C_m(0)$, the $P_m(\tau) < 1$ curves are all differently periodic functions with period T_n , except at resonance. By comparing Figs. 3(a) and 3(c), as resonance is approached, the maximal values of $P_m(\tau)$ for this initial condition are rank-ordered (or decrease monotonically) with m . But at resonance, Fig. 3(e) shows

that the $P_{\pm\frac{1}{2}}(\tau)$ have the largest maxima and are out of phase with each other by $T_n/2$, as are the generally smaller $P_{\pm\frac{3}{2}}(\tau)$ maxima. From Figs. 3(b) and 3(d), it is apparent that as resonance is approached, the $P_m(\tau)$ maxima increase monotonically in the order of decreasing m . However, this changes dramatically at resonance. For both boundary conditions at resonance, $P_{\pm\frac{3}{2}}(\tau)$ and $P_{\pm\frac{1}{2}}(\tau)$ are respectively equivalent functions out of phase with each other by $T_n/2$, and the periodicity of the points of equality of the four curves is again $T_n/2$. But at resonance in Fig. 3(f), the equivalent $P_{\pm\frac{3}{2}}(\tau)$ alternate between 0 and 1, and are out of phase by $T_n/2$ with each other, and the usually smaller equivalent $P_{\pm\frac{1}{2}}(\tau)$ alternate between 0 and $\frac{3}{8}$ and are also out of phase with each other by $T_n/2$. This figure also applies for $J = \frac{3}{2}$ with m , $P_m(\tau)$, $C_m(0)$ and T_n replaced by \bar{m} , $P_{\bar{m}}(\tau)$, $D_{\bar{m}}(0)$, and T_e , respectively.

In Fig. 4, the analogous $P_m(\tau)$ curves for $I = 2$ are shown. For the cases of the occupations of each state being initially equally probable, Figs. 4(a) and 4(c) show that away from resonance, the maximal values of $P_m(\tau)$ either decrease monotonically with m or saturate at their initial values. However, at resonance this changes dramatically. Fig. 4(e) shows that at resonance, $P_0(\tau) \leq 1$ has the largest maximal value. The τ points of equal probability are again 0, $\frac{1}{2}$ and 1. The $P_{\pm m}(\tau)$ for $m \neq 0$ are equivalent curves that are $T_n/2$ out of phase with each other. In comparing the right column Figs. 4(b) and 4(d), it is clear that in each of these integer I cases, as resonance is approached, the increase in the maximal values of $P_m(\tau)$ occurs monotonically with decreasing m , until at resonance, dramatic changes occur. At resonance, Fig. 4(f) also shows that for $C_I(0) = 1$, the largest maximal $0 \leq P_{\pm I}(\tau) \leq 1$ are equivalent functions that are out of phase by $T_n/2$ with each other, and all of the $P_{\pm m}(\tau)$ for $m \neq 0$ are equivalent to each other but out of phase by $T_n/2$ with each other. The order of their maxima has dramatically changed from a monotonic decrease with m as resonance is approached, to a monotonic decrease with decreasing $|m|$ at resonance, at which the period of $P_0(\tau)$ abruptly changes to $T_n/2$. This figure also applies for $J = 2$ with m , $P_m(\tau)$, $C_m(0)$ and T_n replaced by \bar{m} , $P_{\bar{m}}(\tau)$, $D_{\bar{m}}(0)$, and T_e , respectively.

There are an infinite number of possible initial conditions, even for $I, J = \frac{1}{2}$, since the only condition upon the initial eigenstate occupation probabilities is Eq. (61), so that the phases of each of the $C_m(0)$ or $D_{\bar{m}}(0)$ are arbitrary. No textbooks solved any case other than $I = \frac{1}{2}$, and usually set one of the $C_{\pm\frac{1}{2}}(0) = 0$ or $D_{\pm\frac{1}{2}}(0) = 0$ [15, 16, 24], so that the relative phases of the two states were irrelevant. But as seen in the left panels of Fig. 1, the relative phases of the $C_{\pm\frac{1}{2}}(0)$ or $D_{\pm\frac{1}{2}}(0) = 0$ are indeed relevant and measurable.

It is interesting to show the results for $C_0(0) = 1$ or $D_0(0) = 1$ in the cases of integral I or J . In Figs. 5 and 6, we show the four cases of $C_0(0) = 1$ or $D_0(0) = 1$ for $I = 1, 2, 3$, and 4. Figures 5(a), 5(c), and 5(e) show

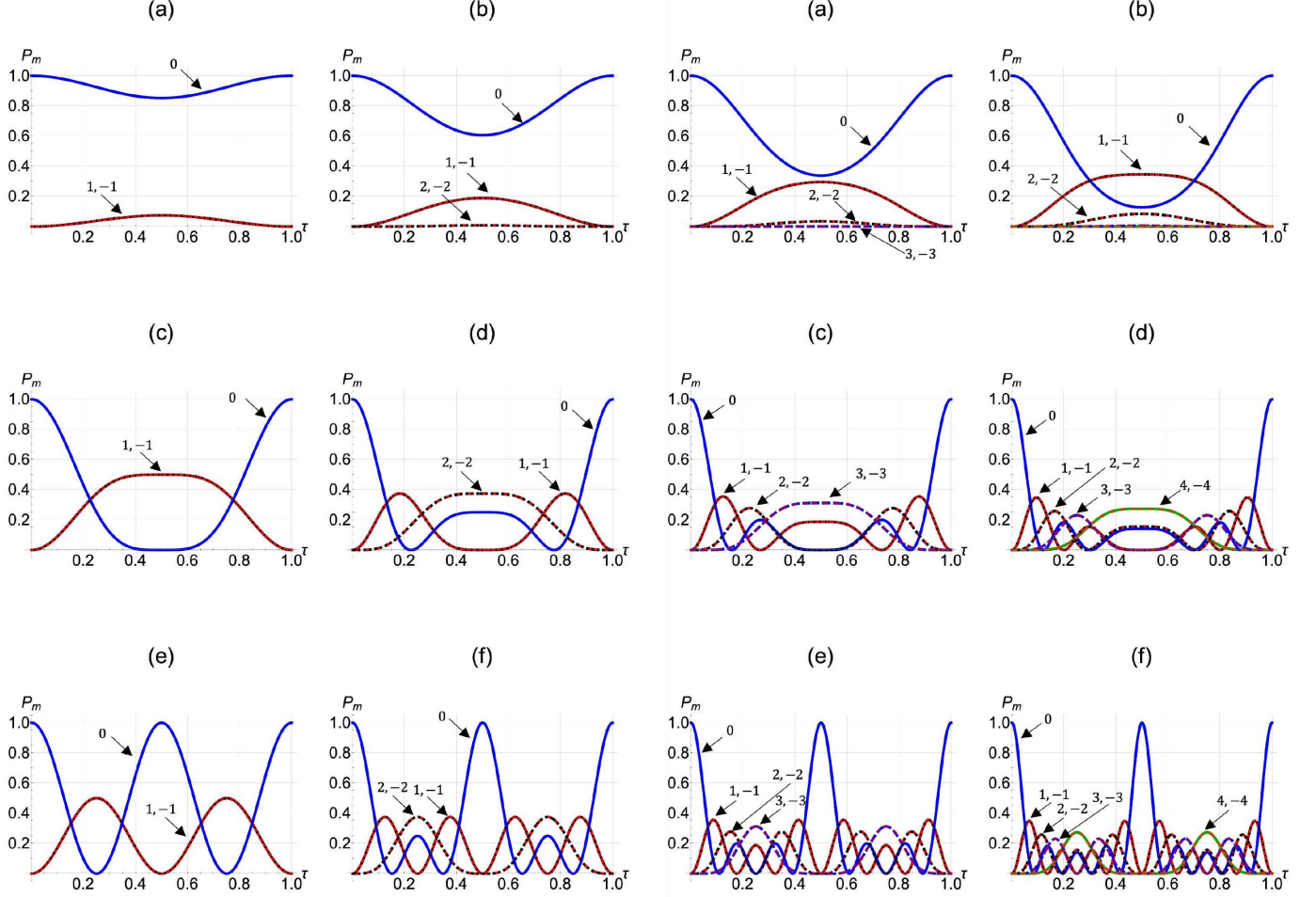


FIG. 5. (Color online) Plots of $P_m(\tau)$ for $0 \leq \tau = t/T_n \leq 1$. (a), (c), (e): $I = 1$. (b), (d), (f): $I = 2$. In both cases $C_0(0) = 1$. Plots of $P_0(\tau)$ (solid blue), $P_1(\tau)$ (solid red), and $P_{-1}(\tau)$ (dot-dashed black). For $I = 2$, $P_2(\tau)$ (dashed red), and $P_{-2}(\tau)$ (dotted black). In (a) and (b), $\omega/\omega_{n0} = 0.95$, in (c) and (d), $\omega/\omega_{n0} = 0.99$, and in (e) and (f), $\omega/\omega_{n0} = 1$. This figure also applies for $J = 1, 2$ with $\tau = t/T_e$ and m , ω_{n0} , and $C_m(0)$ respectively replaced by \bar{m} , ω_{e0} , and $D_{\bar{m}}(0)$.

the analogous cases with $C_0(0) = 1$ or $D_0(0) = 1$ for $I, J = 1$, Figs. 5(b), 5(d), and 5(f) are for $C_0(0) = 1$ or $D_0(0) = 1$ and $I, J = 2$, and the analogous cases for $I, J = 3$ and 4 are in Figs. 6(a), 6(c), 6(e), and 6(b), 6(d), and 6(f). In each of these cases, regardless of the proximity to resonance, the $P_{\pm m}(\tau)$ or $P_{\pm \bar{m}}(\tau)$ are exactly the same for all $m, \bar{m} \neq 0$ for integral I, J from 1 to 4. On the approach to resonance, the amplitudes of $P_{\pm m}(\tau)$ or $P_{\pm \bar{m}}(\tau)$ increase monotonically with $|m|$ or $|\bar{m}|$. But at resonance, the behaviors of the maxima of $P_{\pm m}(\tau)$ or $P_{\pm \bar{m}}(\tau)$ are generally non-monotonic with $|m|$ or $|\bar{m}|$. One special case is shown in Fig. 6(f). In this case, the identical resonant $P_{\pm 1}(\tau)$ are periodic with period $T_{n,e}/4$. All of the other curves have identical resonant $P_{\pm m}(\tau)$ that are periodic with period $T_{n,e}/2$. Also,

FIG. 6. (Color online) Plots of $P_m(\tau)$ for $0 \leq \tau = t/T_n \leq 1$. (a), (c), (e): $I = 3$. (b), (d), (f): $I = 4$. In both cases $C_0(0) = 1$. Plots of $P_0(\tau)$ (solid blue), $P_1(\tau)$ (solid red), and $P_{-1}(\tau)$ (dot-dashed black), $P_2(\tau)$ (dashed red), $P_{-2}(\tau)$ (dotted black), $P_3(\tau)$ (dashed blue), $P_{-3}(\tau)$ (dotted red). For $I = 4$, $P_4(\tau)$ (solid green) and $P_{-4}(\tau)$ (dashed orange). In (a) and (b), $\omega/\omega_{n0} = 0.95$, in (c) and (d), $\omega/\omega_{n0} = 0.99$, and in (e) and (f), $\omega/\omega_{n0} = 1$. This figure also applies for $J = 3, 4$ with $\tau = t/T_e$ and m , ω_{n0} , and $C_m(0)$ respectively replaced by \bar{m} , ω_{e0} , and $D_{\bar{m}}(0)$.

the order of the decreasing resonant maxima for $I, J = 1$ is $\max[P_0(\tau)] = 1 > \max[P_{\pm 1}(\tau)] = \frac{1}{2}$, for $I, J = 2$ it is $\max[P_0(\tau)] = 1 > \max[P_{\pm 1}(\tau)] = \max[P_{\pm 2}(\tau)] = \frac{3}{8}$, for $I, J = 3$ it is $\max[P_0(\tau)] = 1 > \max[P_{\pm 1}(\tau)] > \max[P_{\pm 3}(\tau)] > \max[P_{\pm 2}(\tau)]$, and for $I, J = 4$ it is $\max[P_0(\tau)] = 1 > \max[P_{\pm 1}(\tau)] > \max[P_{\pm 4}(\tau)] > \max[P_{\pm 3}(\tau)] > \max[P_{\pm 2}(\tau)]$, which are non-monotonic.

B. Period-averaged occupation probabilities near to resonance

For clarity near to resonance, it is useful to compare the time averages of the occupation probabilities given by

$$\overline{P}_{m,\overline{m}} = \frac{1}{T_{n,e}} \int_0^{T_{n,e}} P_{m,\overline{m}}(t) dt \quad (67)$$

in the vicinity of $\omega/\omega_{n,e0} \approx 1$. In Figs. 7-10, we present four near-resonant cases for each I, J value satisfying $\frac{1}{2} \leq I, J \leq 2$. For each figure, subfigure (a) contains plots of the $\overline{P}_{m,\overline{m}}$ for the cases of equal $C_m(0) = \frac{1}{\sqrt{2I+1}}$ or $D_{\overline{m}}(0) = \frac{1}{\sqrt{2J+1}}$, subfigure (b) contains plots of the $\overline{P}_{m,\overline{m}}$ for the cases $C_I(0) = e^{-i(\pi/2+0.2)}/\sqrt{2I+1}$ for $m = I$ or $D_J(0) = e^{-i(\pi/2+0.2)}/\sqrt{2J+1}$ for $\overline{m} = J$ and $C_m(0) = \frac{1}{\sqrt{2I+1}}$ for $m \neq I$ or $D_{\overline{m}}(0) = \frac{1}{\sqrt{2J+1}}$ for $\overline{m} \neq J$, and subfigure (c) contains plots of the $\overline{P}_{m,\overline{m}}$ for the cases $C_m(0) = e^{i\phi_m}/\sqrt{2I+1}$ or $D_{\overline{m}}(0) = e^{i\phi_{\overline{m}}}/\sqrt{2J+1}$, where each of the ϕ_m or $\phi_{\overline{m}}$ are random numbers between 0 and 2π . In each subfigure (d), the plots the $\overline{P}_{m,\overline{m}}$ for the initial case $C_I(0) = 1$ or $D_J(0) = 1$ and the $C_m(0) = 0$ for $m \neq I$ or $D_{\overline{m}}(0) = 0$ for $\overline{m} \neq J$ are shown. In Fig. 7 the $\overline{P}_{m,\overline{m}}$ are plotted over the range $0.95 \leq \omega/\omega_{n,e0} \leq 1.05$, and in Figs. 8-10, $\overline{P}_{m,\overline{m}}$ is plotted over the range $0.99 \leq \omega/\omega_{n,e0} \leq 1.01$. Additional figures for $\frac{5}{2} \leq I, J \leq \frac{9}{2}$ are shown in the Supplementary Material[76].

In Fig. 7, four cases for $I, J = \frac{1}{2}$ are presented. In Fig. 7(a), the initial condition $C_{\frac{1}{2}}(0) = C_{-\frac{1}{2}}(0)$ or $D_{\frac{1}{2}}(0) = D_{-\frac{1}{2}}(0)$ leads near resonance to $\overline{P}_{\frac{1}{2}}(\omega/\omega_{n,e0}) \geq \overline{P}_{-\frac{1}{2}}(\omega/\omega_{n,e0})$, the equality only holding at resonance, $\omega = \omega_{n,e0}$. For $C_{\frac{1}{2}}(0) = e^{-i(\pi/2+0.2)}C_{-\frac{1}{2}}(0)$ or $D_{\frac{1}{2}}(0) = e^{-i(\pi/2+0.2)}D_{-\frac{1}{2}}(0)$, the near-resonant $\overline{P}_{\pm\frac{1}{2}}(\omega/\omega_{n,e0})$ curves shown in Fig. 7(b) are nearly inverted with respect to the curves shown in Fig. 7(a), although a close examination of the vertical scales reveals that the inverted curves in Fig. 7(b) are numerically distinct from those in Fig. 7(a), except at resonance. With randomly chosen different initial $C_m(0)$ phases ϕ_m or $D_{\overline{m}}(0)$ phases $\phi_{\overline{m}}$, the curves shown in Fig. 7(c) are nearly identical to those shown in Fig. 7(b), but the magnitudes of the curves are again different in the two figures, except exactly at resonance. In Fig. 7(d) for $C_{-\frac{1}{2}} = 0$ or $D_{-\frac{1}{2}} = 0$, $\overline{P}_{\frac{1}{2}} \gg \overline{P}_{-\frac{1}{2}}$, except very close to resonance, at which $\overline{P}_{\frac{1}{2}} = \overline{P}_{-\frac{1}{2}}$.

The analogous cases for $I, J = 1$ are shown in Fig. 8. For all of the $C_m(0) = \frac{1}{\sqrt{3}}$, $\overline{P}_1(\omega/\omega_{n,e0}) > \overline{P}_0(\omega/\omega_{n,e0}) > \overline{P}_{-1}(\omega/\omega_{n,e0})$, except very near to resonance, as shown in Fig. 8(a). At resonance, $\overline{P}_0(1) > \overline{P}_1(1) = \overline{P}_{-1}(1)$. However, when either $C_1(0) = e^{-i(\pi/2+0.2)}\frac{1}{\sqrt{3}}$ and $C_0(0) = C_{-1}(0) = \frac{1}{\sqrt{3}}$, or $D_1(0) = e^{-i(\pi/2+0.2)}\frac{1}{\sqrt{3}}$ and $D_0(0) =$

$D_{-1}(0) = \frac{1}{\sqrt{3}}$ away from resonance, $\overline{P}_0(\omega/\omega_{n,e0}) > \overline{P}_1(\omega/\omega_{n,e0}) > \overline{P}_{-1}(\omega/\omega_{n,e0})$, except very near to resonance, at which $\overline{P}_1(1) = \overline{P}_{-1}(1) > \overline{P}_0(1)$, as shown in Fig. 8(b). For the particular initial condition example of equal amplitudes and random phases of either the $C_m(0)$ or $D_{\overline{m}}(0)$ shown in Fig. 8(c), sufficiently far from resonance, $\overline{P}_0(\omega/\omega_{n,e0}) > \overline{P}_{-1}(\omega/\omega_{n,e0}) > \overline{P}_1(\omega/\omega_{n,e0})$, and at resonance, $\overline{P}_0(1) > \overline{P}_1(1) = \overline{P}_{-1}(1)$. For the case of either $C_1(0) = 1$ or $D_1(0)$ shown in Fig. 8(d), $\overline{P}_1(\omega/\omega_{n,e0}) \gg \overline{P}_0(\omega/\omega_{n,e0}) \gg \overline{P}_{-1}(\omega/\omega_{n,e0})$, except very close to resonance, at which $\overline{P}_1(1) = \overline{P}_{-1}(1) > \overline{P}_0(1)$. We note that the functional dependencies of either the $\overline{P}_m(\omega/\omega_{n,e0})$ or the $\overline{P}_{\overline{m}}(\omega/\omega_{n,e0})$ are distinctly different in Fig. 8(d) from the respective forms in Figs. 8(a) to 8(c). In other words, the same figures and statements for $J = 1$ apply by replacing $C_m(0)$ with $D_{\overline{m}}(0)$ and ω_{n0} with ω_{e0} .

Figure 9 presents the corresponding figures for $I, J = \frac{3}{2}$. At resonance, Figs. 9(a), 9(b), and 9(c) all show $\overline{P}_{\frac{1}{2}}(1) = \overline{P}_{-\frac{1}{2}}(1) > \overline{P}_{\frac{3}{2}}(1) = \overline{P}_{-\frac{3}{2}}(1)$. Although in Fig. 9(a), the behavior at $\omega/\omega_{n,e0} = 1 \pm 0.01$ (the edges of the figure) is monotonic in m or \overline{m} in $\overline{P}_{m,\overline{m}}(\omega/\omega_{n,e0})$ with $\overline{P}_{\frac{3}{2}}(\omega/\omega_{n,e0}) > \overline{P}_{\frac{1}{2}}(\omega/\omega_{n,e0}) > \overline{P}_{-\frac{1}{2}}(\omega/\omega_{n,e0}) > \overline{P}_{-\frac{3}{2}}(\omega/\omega_{n,e0})$, that monotonicity in m or \overline{m} is not present in Figs. 9(b) and 9(c). Thus the phases of the initial amplitudes modify the non-resonant results substantially. In addition, Fig. 9(d) shows that either for $C_{\frac{3}{2}}(0) = 1$ or for $D_{\frac{3}{2}}(0) = 1$, sufficiently away from resonance, $\overline{P}_{\frac{3}{2}}(\omega/\omega_{n,e0}) > \overline{P}_{\frac{1}{2}}(\omega/\omega_{n,e0}) > \overline{P}_{-\frac{1}{2}}(\omega/\omega_{n,e0}) > \overline{P}_{-\frac{3}{2}}(\omega/\omega_{n,e0})$, which is also monotonic in either m or \overline{m} , but at resonance, $\overline{P}_{\frac{3}{2}}(1) = \overline{P}_{-\frac{3}{2}}(1) > \overline{P}_{\frac{1}{2}}(1) = \overline{P}_{-\frac{1}{2}}(1)$, opposite to the resonant behavior shown in Fig. 9(a).

The corresponding figures for $I, J = 2$ are presented in Fig. 10. At resonance, $\overline{P}_0(1) > \overline{P}_1(1) = \overline{P}_{-1}(1) > \overline{P}_2(1) = \overline{P}_{-2}(1)$ in Figs. 10(a), and 10(b), but that order is not obeyed at resonance in Fig. 10(c), unlike the behavior in Fig. 9(c) for $I, J = \frac{3}{2}$. As for the monotonicity in either m or \overline{m} at $\omega/\omega_{n,e0} = 1 \pm 0.01$, Figs. 10(a) and 10(d) both display $\overline{P}_2(\omega/\omega_{n,e0}) > \overline{P}_1(\omega/\omega_{n,e0}) > \overline{P}_0(\omega/\omega_{n,e0}) > \overline{P}_{-1}(\omega/\omega_{n,e0}) > \overline{P}_{-2}(\omega/\omega_{n,e0})$, but as in Figs. 9(b) and 9(c), that monotonicity at those values away from resonance are not present in Figs. 10(b) and 10(c). In addition, at resonance, Fig. 10(d) shows for either $C_2(0) = 1$ or $D_2(0)$ that $\overline{P}_2(1) = \overline{P}_{-2}(1) > \overline{P}_1(1) = \overline{P}_{-1}(1) > \overline{P}_0(1)$, in analogy with Fig. 5(d).

VI. PERTURBATIONS ABOUT THE BARE HAMILTONIAN

For nuclei with $I \geq 1$, the nuclear electric quadrupole moment can exist [3, 13, 50], and in many cases, can dramatically broaden the NMR transitions. This is especially true for ^{14}N , which has a 99.6% natural abundance, but it has been particularly difficult to observe in molecules with standard NMR techniques until rather

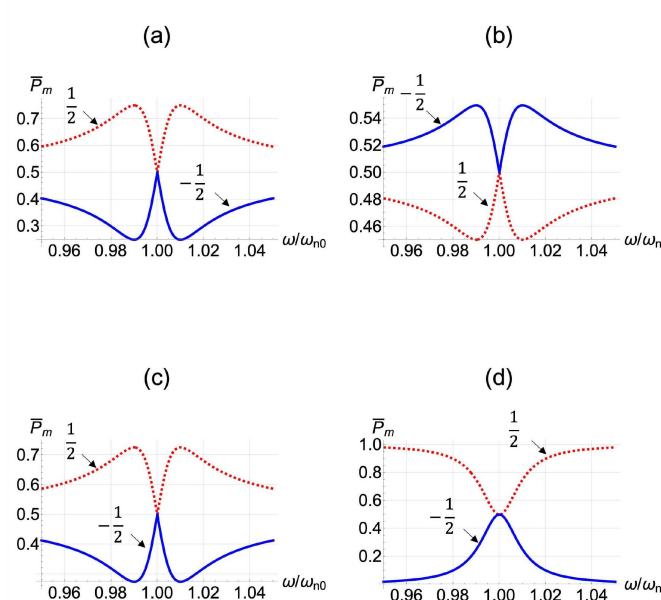


FIG. 7. Plots of $\bar{P}_m(\omega/\omega_{n0})$ for $I = \frac{1}{2}$ and $0.95 \leq \omega/\omega_{n0} \leq 1.05$. $m = \frac{1}{2}$: (dotted red), and $m = -\frac{1}{2}$: (solid blue). This figure also applies for $J = \frac{1}{2}$ with m and ω_{n0} respectively replaced by \bar{m} and ω_{e0} .

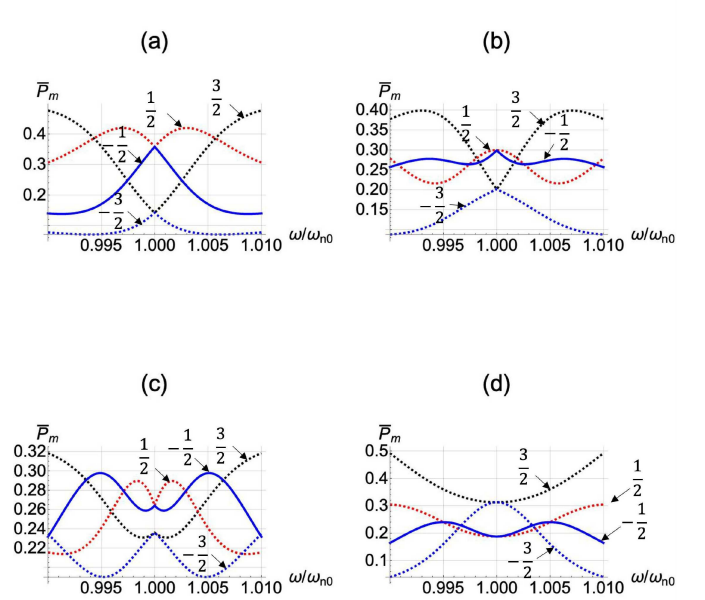


FIG. 9. Plots of $\bar{P}_m(\omega/\omega_{n0})$ for $I = \frac{3}{2}$ and $0.99 \leq \omega/\omega_{n0} \leq 1.01$. $m = \frac{3}{2}$: (dotted black), $m = \frac{1}{2}$: (dotted red), $m = -\frac{1}{2}$: (solid blue), and $m = -\frac{3}{2}$: (dotted blue). This figure also applies for $J = \frac{3}{2}$ with m and ω_{n0} respectively replaced by \bar{m} and ω_{e0} .

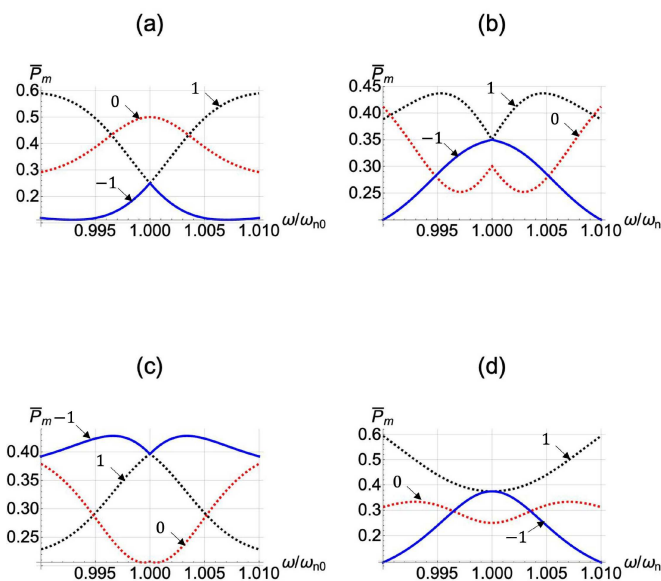


FIG. 8. Plots of $\bar{P}_m(\omega/\omega_{n0})$ for $I = 1$ and $0.99 \leq \omega/\omega_{n0} \leq 1.01$. $m = 1$: (dotted black), $m = 0$: (dotted red), and $m = -1$: (solid blue). This figure also applies for $J = 1$ with m and ω_{n0} respectively replaced by \bar{m} and ω_{e0} .

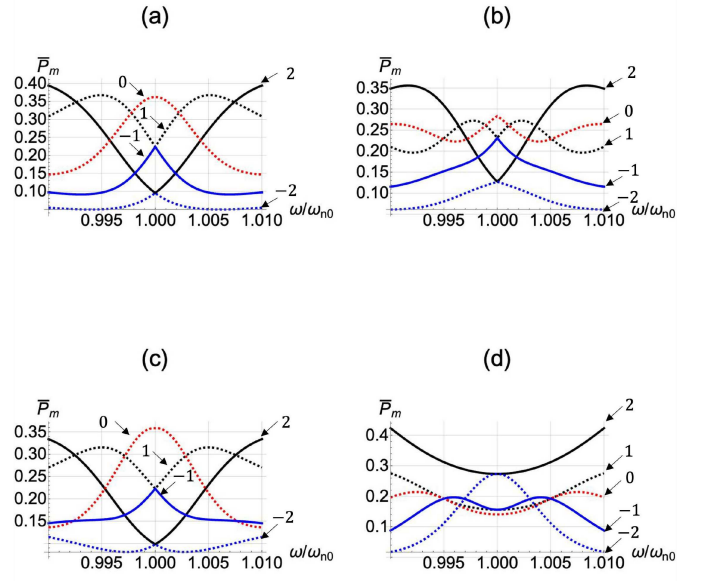


FIG. 10. Plots of $\bar{P}_m(\omega/\omega_{n0})$ for $I = 2$ and $0.99 \leq \omega/\omega_{n0} \leq 1.01$. $m = 2$: (solid black), $m = 1$: (dotted black), $m = 0$: (dotted red), $m = -1$: (solid blue), and $m = -2$: (dotted blue). This figure also applies for $J = 2$ with m and ω_{n0} respectively replaced by \bar{m} and ω_{e0} .

recently, when the sample was dissolved in a variety of solvents [52–55]. However, ^{14}N is an essential isotope in the constituent organic molecules adenine, cytosine, guanine, and thymine of deoxyribonucleic acid (DNA). Table I contains a list of the dipole and quadrupole moments and the nuclear spin and parity values for the elemental constituents of those molecules, as well as the chemically possible defect isotopes, along with some other isotopes relevant for vertebrates, particularly for humans. In the first-row atoms [4, 5, 7–9], the interaction of the electrons with the nucleus gives rise to hyperfine structure in the electronic atomic structure. Hund's rules for the electronic state hieroglyphic notation $^{2S+1}\text{L}_J$, [24, 26] along with the overall antisymmetry of the electronic states for an odd number of electrons, indicate that for only filled $n = 1$ and partially filled $n = 2$ atomic level states, the electronic ground state of atomic N is $^4\text{S}_{\frac{1}{2}}$, and excited states successively higher in energy are $^2\text{D}_{\frac{3}{2}}$, $^2\text{D}_{\frac{5}{2}}$, $^2\text{P}_{\frac{1}{2}}$, $^2\text{P}_{\frac{3}{2}}$, and $^2\text{S}_{\frac{1}{2}}$. Thus, there are 6 low-lying electronic states of N with $J = \frac{5}{2}, \frac{3}{2}$, and $\frac{1}{2}$.

Thus, for atoms, one can treat the low-lying states accurately by assuming the electronic parts of their nuclear moments can be treated by their J values, and rank-ordered in terms of their energies. Of course in molecules such as adenine, cytosine, guanine, and thymine, with multiple C, N, O, and H atoms, one might question whether the overall molecular structure could have a quantized angular momentum. We will return to this question in the following.

The nuclear electric quadrupole moment for $I \geq 1$ in atoms contains terms proportional to the three electric field gradients, $\frac{\partial E}{\partial x_i}$, which are highly anisotropic. This was treated perturbatively using the standard interaction representation starting with the time-independent magnetic field Hamiltonian $H_0 = \mu_N I_z$ [56]. However, as Gottfried emphasized, such treatments cannot possibly work at or near to resonance [15].

For atoms, we assume that the nuclear total angular momentum states $|I, m\rangle$ with $-I \leq m \leq I$ and operators \mathbf{I}^2 and I_z satisfy Eq. (2), with $-I \leq m \leq I$, and the analogous electronic states $|J, \overline{m}\rangle$ with $-J \leq \overline{m} \leq J$ satisfy

$$\mathbf{J}^2|J, \overline{m}\rangle = \hbar^2 J(J+1)|J, \overline{m}\rangle, \quad (68)$$

$$J_z|J, \overline{m}\rangle = \overline{m}\hbar|J, \overline{m}\rangle, \quad (69)$$

and the J_i operators obey the Lie algebra, Eq. (2), and are independent of the nuclear I_j operators, as has commonly been assumed in the literature [4, 5, 7–9]. In early atomic hyperfine structure calculations of the first row atoms, the electronic total angular momentum \mathbf{J} is coupled to the nuclear spin \mathbf{I} in powers of $\mathbf{I} \cdot \mathbf{J}$ [4, 5, 7–9]. The nuclear-electronic magnetic dipole, electric quadrupole, and magnetic octupole interactions may be written as

the scalar operators

$$H_D = A(I, J)\mathbf{I} \cdot \mathbf{J}/\hbar^2, \quad (70)$$

$$H_Q = B(I, J)\left[(\mathbf{I} \cdot \mathbf{J}/\hbar^2)^2 + \frac{1}{2}(\mathbf{I} \cdot \mathbf{J}/\hbar^2) - \frac{1}{3}I(I+1)J(J+1)\right], \quad (71)$$

$$H_O = C(I, J)\left[(\mathbf{I} \cdot \mathbf{J}/\hbar^2)^3 + 2(\mathbf{I} \cdot \mathbf{J}/\hbar^2)^2 + \frac{1}{5}(\mathbf{I} \cdot \mathbf{J}/\hbar^2)[-3I(I+1)J(J+1) + I(I+1) + J(J+1) + 3] - 5I(I+1)J(J+1)\right], \quad (72)$$

which are respectively proportional to linear, quadratic, and cubic functions of $(\mathbf{I} \cdot \mathbf{J})$, where $A(I, J)$, $B(I, J)$, and $C(I, J)$ are energies that are real functions of I and J respectively proportional to the nuclear magnetic dipole, electric quadrupole, and magnetic octupole moments that separately contain the integrations over the nuclear and electronic structural variables in the $|I, I\rangle \times |J, J\rangle$ state that factor due to the Wigner-Eckart theorem [3, 5, 13, 25]. Similarly the electric hexadecapole moment can be written as a quartic function of $(\mathbf{I} \cdot \mathbf{J})$ [3, 5, 25]. Hence, in the absence of such moments, there is a separation of the electronic and the nuclear quantum variables, and at least for atoms, the couplings are proportional to powers of $\mathbf{I} \cdot \mathbf{J}$. Thus for atoms, it has been standard to treat the overall electronic spin with the quantum operator \mathbf{J} , which is entirely analogous to the nuclear spin operator \mathbf{I} .

We note that the nuclear moment perturbations were studied in the absence of an applied magnetic field long ago to include their effects upon the atomic hyperfine structure of atoms [4, 5, 7–9]. In those cases, the operators \mathbf{I} and \mathbf{J} , as well as the combined $\mathbf{F} = \mathbf{I} + \mathbf{J}$ gave good quantum numbers, and the nuclear moment perturbations could be written in terms of the single quantum number $K = F(F+1)$ [4, 5, 7–9]. However, with the three-component applied magnetic fields, that symmetry is completely broken in all three directions, but the scalar operator $\mathbf{I} \cdot \mathbf{J}$ is well defined, provided that I and J are both good quantum numbers.

Thus, starting with the bare Hamiltonians for the nuclei and the electronic cloud of an atom, we assume the total Hamiltonian can be written as

$$\hat{H}_{ne}(t) = \hat{H}_n(t) \otimes \mathbf{1}_e + \mathbf{1}_n \otimes \hat{H}_e(t) + \delta\hat{V}_{ne}, \quad (73)$$

$$\hat{H}_n(t) = \hat{H}_n^0(t) + \hat{V}_n(t), \quad (74)$$

$$\hat{H}_e(t) = \hat{H}_e^0(t) + \hat{V}_e(t), \quad (75)$$

$$\delta\hat{V}_{ne} = \sum_{q=0}^{2I} K_q [\mathbf{I} \cdot \mathbf{J}/\hbar^2]^q \mathbf{1}_n \otimes \mathbf{1}_e, \quad (76)$$

where $\mathbf{1}_n$ and $\mathbf{1}_e$ are identity matrices of respective ranks $2I+1$ and $2J+1$, the K_q are real functions of I, J , and the starting (or bare) Hamiltonian consists of $\hat{H}_n^0(t)$ given by Eq. (4) and $\hat{H}_e^0(t)$ given by Eq. (45).

We note that $|\psi_{ne}(t)\rangle$ contains components of the vector operators \mathbf{I} and \mathbf{J} , which can respectively be represented by a matrices of rank $2I+1$ and $2J+1$ that operate on the nuclear and electronic angular momentum subspaces of those ranks. The matrix representation of the combined Hamiltonian $\hat{H}_{ne}(t)$ presented in the following is a $(2I+1) \times (2I+1)$ matrix representing the nuclear spin I states multiplied by an independent $(2J+1) \times (2J+1)$ matrix representing the electronic angular momentum J states, and $|\psi_{ne}(t)\rangle$ is a rank $2I+2J+2$ column vector in Nambu representation, the upper $2I+1$ and lower $2J+1$ elements are acted upon by the respective independent rank $2I+1$ and $2J+1$ nuclear and electronic Hamiltonian matrix forms.

It is then easy to show that the above bare $|\psi_{ne}^0(t)\rangle$ for the electrons and nuclei in atoms satisfies the Schrödinger equation for the full Hamiltonian,

$$\begin{aligned}\hat{H}_{ne}^0(t) &= \hat{H}_n^0(t) \otimes \mathbf{1}_e \\ &\quad + \mathbf{1}_n \otimes \hat{H}_e^0(t),\end{aligned}\quad (77)$$

$$i\hbar \frac{\partial}{\partial t} |\psi_{ne}^0(t)\rangle = \hat{H}_{ne}^0(t) |\psi_{ne}^0(t)\rangle. \quad (78)$$

Thus, we therefore consider two types of perturbations $\hat{V}(t)$: those that are variations in the explicit periodic time-dependence of the actual experimental applied magnetic field, and those that are time-independent natural nuclear moment perturbations that couple the nuclear spin operator \mathbf{I} with the surrounding electronic spin operator \mathbf{J} .

Depending upon the type of experiment, there will be a time-dependent perturbation of the difference between the experimental time-dependent field and the RWA time-dependent field. These effect both the nuclei and the electrons. For a general time-periodic field form in the \mathbf{x} direction, we have

$$\delta\hat{V}_1(t) = \delta\hat{V}_{n1}(t) \otimes \mathbf{1}_e + \mathbf{1}_n \otimes \delta\hat{V}_{e1}(t), \quad (79)$$

$$\delta\hat{V}_{n1}(t) = -\omega_{n1} I_y \sin(\omega t) + \omega_{n1} I_x \sum_{p=2}^{\infty} a_p \cos[p\omega(t - t_0)], \quad (80)$$

$$\delta\hat{V}_{e1}(t) = -\omega_{e1} J_y \sin(\omega t) + \omega_{e1} J_x \sum_{p=2}^{\infty} a_p \cos[p\omega(t - t_0)], \quad (81)$$

where any wave form can be calculated using standard Fourier series techniques [57].

For the magic-angle spinning case [58], we have

$$\delta\hat{V}_2(t) = \delta\hat{V}_{n2}(t) \otimes \mathbf{1}_e + \mathbf{1}_n \otimes \delta\hat{V}_{e2}(t), \quad (82)$$

$$\delta\hat{V}_{n2}(t) = 2\omega_{n1} \sin \theta \cos(\omega t) (I_z \cos \theta - I_x \sin \theta), \quad (83)$$

$$\delta\hat{V}_{e2}(t) = 2\omega_{e1} \sin \theta \cos(\omega t) (J_z \cos \theta - J_x \sin \theta). \quad (84)$$

For each of the two experiments $i = 1, 2$, the full perturbation that includes the nuclear moments and either of

these time-dependent experiments may then be written as

$$\delta\hat{V}_i(t) = \delta\hat{V}_{ni}(t) \otimes \mathbf{1}_e + \mathbf{1}_n \otimes \delta\hat{V}_{ei}(t) + \delta\hat{V}_{n,e}, \quad (85)$$

$$\delta\hat{V}_{n,e} = \sum_{q=0}^{2I} K_q (\mathbf{I} \cdot \mathbf{J} / \hbar^2)^q \mathbf{1}_n \otimes \mathbf{1}_e, \quad (86)$$

where $i = 1, 2$ for the two experiments and the K_q are functions of the quantum numbers I and J and of the various constants for the nuclear moment and electronic wave functions evaluated in the $|I, I\rangle$ and $|J, J\rangle$ states according to the Wigner-Eckart theorem [5]. All of the interactions between the nuclei and electrons in an atom, from the magnetic dipole, electric quadrupole, magnetic octupole, electric hexadecapole, etc., etc., are all fully represented by Eq. (86). We note that $\mathbf{I} \cdot \mathbf{J}$ is a scalar operator [4, 5, 7–9].

We are now ready to calculate the perturbations due to $\lambda \delta\hat{V}_i(t)$, each of which is assumed proportional to the dummy variable λ . Letting

$$\begin{aligned}|\psi_{ne}(t)\rangle &= |\psi_{RWA,ne}(t)\rangle + \lambda |\psi_{1,ne}(t)\rangle \\ &\quad + \lambda^2 |\psi_{2,ne}(t)\rangle + \dots,\end{aligned}\quad (87)$$

$$\hat{H}_{ne}(t) = \hat{H}_{RWA,ne}(t) + \lambda \delta\hat{V}_i(t), \quad (88)$$

and requiring that the Schrödinger equation be satisfied in each order ℓ of λ ,

$$i\hbar \frac{\partial}{\partial t} |\psi_{\ell,ne}(t)\rangle = \hat{H}_{ne}(t) |\psi_{\ell,ne}(t)\rangle, \quad (89)$$

we have to $\mathcal{O}(\lambda^0)$ that

$$i\hbar \frac{\partial}{\partial t} |\psi_{ne}^0(t)\rangle = \hat{H}_{ne}^0(t) |\psi_{ne}^0(t)\rangle. \quad (90)$$

To $\mathcal{O}(\lambda)$, we have to satisfy

$$i\hbar \frac{\partial}{\partial t} |\psi_{1,ne}(t)\rangle = \hat{H}_{ne}^0(t) |\psi_{1,ne}(t)\rangle + \delta\hat{V}_i(t) |\psi_{ne}^0(t)\rangle, \quad (91)$$

and to $\mathcal{O}(\lambda^\ell)$ where $\ell \geq 1$ is an integer, the equation to satisfy is

$$i\hbar \frac{\partial}{\partial t} |\psi_{\ell,ne}(t)\rangle = \hat{H}_{ne}^0(t) |\psi_{\ell,ne}(t)\rangle + \delta\hat{V}_i(t) |\psi_{\ell-1,ne}(t)\rangle. \quad (92)$$

We first transform the expression to $\mathcal{O}(\lambda^0)$, Eq. (90). We write

$$\begin{aligned}e^{i(\beta_n I_y \mathbf{1}_y + \beta_e \mathbf{1}_e + \beta_n J_y)/\hbar} e^{i\omega t(I_z \mathbf{1}_e + \mathbf{1}_n J_z)/\hbar} &\left(i\hbar \frac{\partial}{\partial t} \right) \\ &\times e^{-i\omega t(I_z \mathbf{1}_e + \mathbf{1}_n J_z)/\hbar} e^{-i(\beta_n I_y \mathbf{1}_e + \beta_e \mathbf{1}_n J_y)/\hbar} \\ &\times e^{i(\beta_n I_y \mathbf{1}_e + \beta_e \mathbf{1}_n J_y)/\hbar} e^{i\omega t(I_z \mathbf{1}_e + \mathbf{1}_n J_z)/\hbar} |\psi_{ne}^0(t)\rangle\end{aligned}\quad (93)$$

$$\begin{aligned} &= e^{i(\beta_n I_y \mathbf{1}_e + \beta_e \mathbf{1}_n J_y)/\hbar} e^{i\omega t(I_z \mathbf{1}_e + \mathbf{1}_n J_z)/\hbar} \hat{H}_{ne}^0(t) \\ &\times e^{-i\omega t(I_z \mathbf{1}_e + \mathbf{1}_n J_z)/\hbar} e^{-i(\beta_n I_y \mathbf{1}_e + \beta_e \mathbf{1}_n J_y)/\hbar} \\ &\times e^{i(\beta_n I_y \mathbf{1}_e + \beta_e \mathbf{1}_n J_y)/\hbar} e^{i\omega t(I_z \mathbf{1}_e + \mathbf{1}_n J_z)/\hbar} |\psi_{ne}^0(t)\rangle,\end{aligned}\quad (94)$$

where $\hat{H}_{ne}^0(t)$ is given by Eq. (51). We note that Eq. (94) could be rewritten as

$$i\hbar \frac{\partial}{\partial t} |\tilde{\psi}_{ne}^0(t)\rangle = \hat{H}_{ne}^0(t) |\tilde{\psi}_{ne}^0(t)\rangle, \quad (95)$$

where

$$\begin{aligned} \frac{\partial}{\partial t} &= e^{i(\beta_n I_y \mathbf{1}_e + \beta_e \mathbf{1}_n J_y)/\hbar} e^{i\omega t(I_z \mathbf{1}_e + \mathbf{1}_n J_z)/\hbar} \left(\frac{\partial}{\partial t} \right) \\ &\times e^{-i\omega t(I_z \mathbf{1}_e + \mathbf{1}_n J_z)/\hbar} e^{-i(\beta_n I_y \mathbf{1}_e + \beta_e \mathbf{1}_n J_y)/\hbar}, \end{aligned} \quad (96)$$

$$\begin{aligned} \hat{H}_{ne}^0(t) &= e^{i(\beta_n I_y \mathbf{1}_e + \beta_e \mathbf{1}_n J_y)/\hbar} e^{i\omega t(I_z \mathbf{1}_e + \mathbf{1}_n J_z)/\hbar} \\ &\times \hat{H}_{ne}^0(t) \\ &\times e^{-i\omega t(I_z \mathbf{1}_e + \mathbf{1}_n J_z)/\hbar} e^{-i(\beta_n I_y \mathbf{1}_e + \beta_e \mathbf{1}_n J_y)/\hbar}, \end{aligned} \quad (97)$$

$$\begin{aligned} |\tilde{\psi}_{ne}^0(t)\rangle &= e^{i(\beta_n I_y \mathbf{1}_e + \beta_e \mathbf{1}_n J_y)/\hbar} e^{i\omega t(I_z \mathbf{1}_e + \mathbf{1}_n J_z)/\hbar} \\ &\times |\psi_{ne}^0(t)\rangle, \end{aligned} \quad (98)$$

which is equivalent to the bare Schrödinger equation,

$$i\hbar \frac{\partial}{\partial t} |\tilde{\psi}_{ne}^0(t)\rangle = \hat{H}_0 |\tilde{\psi}_{ne}^0(t)\rangle, \quad (99)$$

where the *time-independent* bare Hamiltonian \hat{H}_0 is given by

$$\hat{H}_0 = \Omega_n I_z \otimes \mathbf{1}_e + \Omega_e \mathbf{1}_n \otimes J_z. \quad (100)$$

From Eqs. (51) and (98), it is evident that

$$\begin{aligned} |\tilde{\psi}_{ne}^0(t)\rangle &= e^{-it(\Omega_n I_z \mathbf{1}_e + \Omega_e \mathbf{1}_n J_z)/\hbar} e^{i(\beta_n I_y \mathbf{1}_e + \beta_e \mathbf{1}_n J_y)/\hbar} \\ &\times |\psi_{ne}^0(0)\rangle \end{aligned} \quad (101)$$

$$= e^{-i\hat{H}_0 t/\hbar} |\psi_{ne,r}^0(0)\rangle_S, \quad (102)$$

where the doubly-rotated time-independent RWF wave function in the Schrödinger picture is

$$|\psi_{ne,r}^0(0)\rangle_S = e^{i(\beta_n I_y \mathbf{1}_e + \beta_e \mathbf{1}_n J_y)/\hbar} |\psi_{ne}^0(0)\rangle. \quad (103)$$

Since the original laboratory frame basis given by Eq. (53) leads to a rather complicated expression for the ground state energy, it is useful to make the change of basis to the doubly-rotated frame in the Schrödinger picture, letting

$$\begin{aligned} |\psi_{ne,r}^0(0)\rangle_S &\equiv \sum_{m=-I}^I \sum_{\bar{m}=-J}^J \tilde{C}_m(0) \tilde{D}_{\bar{m}}(0) \\ &\times |I, m\rangle \otimes |J, \bar{m}\rangle, \end{aligned} \quad (104)$$

where for normalization, we require

$$\sum_{m=-I}^I |\tilde{C}_m(0)|^2 = \sum_{\bar{m}=-J}^J |\tilde{D}_{\bar{m}}(0)|^2 = 1. \quad (105)$$

The coefficients $\tilde{C}_m(0)$ and $\tilde{D}_{\bar{m}}(0)$ in the doubly-rotated new basis are easily seen to be given by

$$\begin{aligned} \tilde{C}_m(0) &= \sum_{m'=-I}^I \langle I, m | e^{i\beta_n I_y/\hbar} | I, m' \rangle C_{m'}(0) \\ &= \sum_{m'=-I}^I d_{m,m'}^{(I)*}(\beta_n) C_{m'}(0), \end{aligned} \quad (106)$$

$$\begin{aligned} \tilde{D}_{\bar{m}}(0) &= \sum_{\bar{m}'=-J}^J \langle J, \bar{m} | e^{i\beta_e J_y/\hbar} | J, \bar{m}' \rangle D_{\bar{m}'}(0) \\ &= \sum_{\bar{m}'=-J}^J d_{\bar{m},\bar{m}'}^{(J)*}(\beta_e) D_{\bar{m}'}(0), \end{aligned} \quad (107)$$

where $d_{m',m}^{(I)}(\beta_n)$ is given in textbooks [16, 24, 27] and explicitly presented in Eq. (42). Of course, $d_{\bar{m},\bar{m}'}^{(J)*}(\beta_e)$ is readily obtained from $d_{m',m}^{(I)}(\beta_n)$ by the appropriate substitutions and complex conjugation.

Then, in this doubly-rotated basis, the energy of a single “non-interacting” state, which only interacts with the applied magnetic field, is

$$\tilde{E}_{ne}^{(0)}(m, \bar{m}) = \hbar(m\Omega_n + \bar{m}\Omega_e), \quad (108)$$

and the most general form of the non-interacting state energy is

$$\tilde{E}_{ne}^{(0)} = \hbar \left(\Omega_n \sum_{m=-I}^I m |\tilde{C}_m(0)|^2 + \Omega_e \sum_{\bar{m}=-J}^J \bar{m} |\tilde{D}_{\bar{m}}(0)|^2 \right). \quad (109)$$

With this change of basis, we are now in the position to use standard perturbation theory [15, 16, 24, 27]. Transforming Eq. (92) as for $\mathcal{O}(\lambda^0)$, we obtain

$$i\hbar \frac{\partial}{\partial t} |\tilde{\psi}_{\ell,ne}(t)\rangle = \tilde{H}_{RWA,ne}(t) |\tilde{\psi}_{\ell,ne}(t)\rangle + \widetilde{\delta\hat{V}_i(t)} |\tilde{\psi}_{\ell-1,ne}(t)\rangle, \quad (110)$$

where

$$\begin{aligned} |\tilde{\psi}_{\ell,ne}(t)\rangle &= e^{-it(\Omega_n I_z \mathbf{1}_e + \Omega_e \mathbf{1}_n J_z)/\hbar} e^{i(\beta_n I_y \mathbf{1}_e + \beta_e \mathbf{1}_n J_y)/\hbar} \\ &\times |\psi_{\ell,ne}(0)\rangle, \end{aligned} \quad (111)$$

$$\begin{aligned} \widetilde{\delta\hat{V}_i(t)} &= e^{i(\beta_n I_y \mathbf{1}_e + \beta_e \mathbf{1}_n J_y)/\hbar} e^{i\omega t(I_z \mathbf{1}_e + \mathbf{1}_n J_z)/\hbar} \delta\hat{V}_i(t) \\ &\times e^{-i\omega t(I_z \mathbf{1}_e + \mathbf{1}_n J_z)/\hbar} e^{-i(\beta_n I_y \mathbf{1}_e + \beta_e \mathbf{1}_n J_y)/\hbar}. \end{aligned} \quad (112)$$

Expressions for the $\widetilde{\delta\hat{V}_i(t)}$ are given in the Appendix.

A. Nuclear moment perturbations in atoms

Recently, there has been an increased interest in the measurement of atomic nuclear moments, with most

of the work being on measurements of the electric quadrupole moment and the magnetic octupole moment [6, 51, 59–75] Hence a new experimental method that could lead to improved accuracy of such moment measurements is presently warranted.

It is easily shown that the untransformed nuclear moment interactions may be written as in Eq. (1),

$$\delta\hat{V}_{ne} = \sum_{q=0}^{2I} K_q (\mathbf{I} \cdot \mathbf{J}/\hbar^2)^q, \quad (113)$$

where

$$\mathbf{I} \cdot \mathbf{J} = I_z J_z + \frac{1}{2}(I_- J_+ + I_+ J_-), \quad (114)$$

and where $J_{\pm} = J_x \pm i J_y$ and $I_{\pm} = I_x \pm i I_y$. Provided that I and J are good quantum numbers, such as for atoms in the absence of the nuclear moment interactions, the entire infinite set of these transformed nuclear moment interactions are independent of t , and can in principle be solved to arbitrary order in time-independent perturbation theory. Then the transformed nuclear moment interactions may be written as

$$\widetilde{\delta\hat{V}_{ne}} = e^{i(\beta_n I_y \mathbf{1}_e + \beta_e \mathbf{1}_n J_y)/\hbar} e^{i\omega t(I_z \mathbf{1}_e + \mathbf{1}_n J_z)/\hbar} \delta\hat{V}_{ne} \times e^{-i\omega t(I_z \mathbf{1}_e + \mathbf{1}_n J_z)/\hbar} e^{-i(\beta_n I_y \mathbf{1}_e + \beta_e \mathbf{1}_n J_y)/\hbar}. \quad (115)$$

Now we treat this perturbation as follows: we first transform $\delta\hat{V}_{ne}$ with respect to the two rotations about the z axis by the same angle $-\omega t$. It is easy to show that

$$e^{i\omega t(I_z \mathbf{1}_e + \mathbf{1}_n J_z)/\hbar} (\mathbf{I} \cdot \mathbf{J}) e^{-i\omega t(I_z \mathbf{1}_e + \mathbf{1}_n J_z)/\hbar} = (\mathbf{I} \cdot \mathbf{J}), \quad (116)$$

which is independent of t . This can be done by generalizing the procedures from Eq. (15) to Eq. (19) for the rotated components of \mathbf{I} to the analogous ones for the components of \mathbf{J} . It is also obviously true that when \mathbf{I} and \mathbf{J} are rotating about the same axis by the same angle, their scalar product is invariant under the rotation. Then one can similarly transform $(\mathbf{I} \cdot \mathbf{J})^2$ by inserting

$$\mathbf{1}_n \otimes \mathbf{1}_e = e^{i\omega t(I_z \mathbf{1}_e + \mathbf{1}_n J_z)/\hbar} e^{-i\omega t(I_z \mathbf{1}_e + \mathbf{1}_n J_z)/\hbar} \quad (117)$$

between the two factors of $(\mathbf{I} \cdot \mathbf{J})$. Thus, all of the transformed nuclear moment interactions are completely independent of the time. Then, the two rotation operator transformations can be applied to the wave functions in the laboratory frame by changing the basis to the doubly-rotated frame.

For the leading non-trivial examples of the measurements of the magnetic dipole, electric quadrupole, and magnetic octupole moments, the first order energy $\tilde{E}_{ne}^{(1)}$ is easiest to evaluate in the doubly-rotated frame, Eq. (104), for which the wave function in the doubly-rotated frame is given by

$$|\tilde{\psi}_{0,ne,r}(0)\rangle = |\psi_{RWA,ne,r}\rangle_S. \quad (118)$$

The first-order perturbation for the nuclear moment interactions may therefore be written as

$$\tilde{E}_{ne}^{(1)} = {}_S\langle\psi_{0,ne,r}(0)|\delta\hat{V}_{ne}|\psi_{0,ne,r}(0)\rangle_S, \quad (119)$$

where $\delta\hat{V}_{ne}$ is given by Eq. (113). Note that the operations of I_z, J_z, I_{\pm} , and J_{\pm} present in Eq. (114) are given by [15, 16, 27]

$$I_z|I, m\rangle = m\hbar|I, m\rangle, \quad (120)$$

$$J_z|J, \overline{m}\rangle = \overline{m}\hbar|J, \overline{m}\rangle \quad (121)$$

$$I_{\pm}|I, m\rangle = \hbar\sqrt{(I \mp m)(I \pm m + 1)}|I, m \pm 1\rangle, \quad (122)$$

$$J_{\pm}|J, \overline{m}\rangle = \hbar\sqrt{(J \mp \overline{m})(J \pm \overline{m} + 1)}|J, \overline{m} \pm 1\rangle \quad (123)$$

To evaluate the perturbation to the energy arising from the magnetic dipole, electric quadrupole, and magnetic octupole moments, we use the doubly-rotated reference frame, so that the bare Hamiltonian \hat{H}_0 is diagonal and independent of t . Then, the $q = 0, 1, 2, 3$ terms in $\delta\hat{V}_{ne}$ can be represented by the rank $2I + 2J + 2$ matrix \hat{M}

with elements

$$\begin{aligned}
(\hat{M})_{m',m}^{\overline{m}',\overline{m}} = & K_0 \delta_{m',m} \delta_{\overline{m}',\overline{m}} + K_1 \left[\delta_{m',m} \delta_{\overline{m}',\overline{m}} m \overline{m} \right. \\
& + \frac{1}{2} \left(\delta_{m',m-1} \delta_{\overline{m}',\overline{m}+1} \alpha_{m,-}^I - \alpha_{\overline{m},+}^J + \right. \\
& \left. + \delta_{m',m+1} \delta_{\overline{m}',\overline{m}-1} \alpha_{m,+}^I + \alpha_{\overline{m},-}^J \right) \left. \right] \\
& + K_2 \left\{ \delta_{m',m} \delta_{\overline{m}',\overline{m}} \left[\overline{m} \overline{m} \left(\overline{m} \overline{m} - \frac{1}{2} \right) \right. \right. \\
& \left. + \frac{1}{2} [I(I+1) - m^2] [J(J+1) - \overline{m}^2] \right] \left. \right\} \\
& + \frac{1}{2} \left(\delta_{m',m-1} \delta_{\overline{m}',\overline{m}+1} \alpha_{m,-}^I - \alpha_{\overline{m},+}^J + [2m\overline{m} + m - \overline{m}] \right. \\
& \left. + \delta_{m',m+1} \delta_{\overline{m}',\overline{m}-1} \alpha_{m,+}^I + \alpha_{\overline{m},-}^J - [2m\overline{m} + \overline{m} - m - 1] \right) \\
& + \frac{1}{4} \left(\delta_{m',m-2} \delta_{\overline{m}',\overline{m}+2} \alpha_{m,-}^I - \alpha_{m-1,-}^I - \alpha_{\overline{m},+}^J + \alpha_{\overline{m}+1,-}^J \right. \\
& \left. + \delta_{m',m+2} \delta_{\overline{m}',\overline{m}-2} \alpha_{m,+}^I + \alpha_{m+1,+}^I + \alpha_{\overline{m},-}^J - \alpha_{\overline{m}-1,-}^J \right) \\
& + K_3 \left\{ \delta_{m',m} \delta_{\overline{m}',\overline{m}} \left(m^3 \overline{m}^3 \right. \right. \\
& \left. + \frac{1}{4} (I-m)(I+m+1)(J+\overline{m})(J-\overline{m}+1) \times \right. \\
& \times [2m\overline{m} + (m+1)(\overline{m}-1)] \\
& \left. + \frac{1}{4} (I+m)(I-m+1)(J-\overline{m})(J+\overline{m}+1) \times \right. \\
& \times [2m\overline{m} + (m-1)(\overline{m}+1)] \\
& \left. + \frac{1}{8} \left\{ \delta_{m',m-1} \delta_{\overline{m}',\overline{m}+1} \alpha_{m,-}^I \alpha_{\overline{m},+}^J \left[4m^2 \overline{m}^2 \right. \right. \right. \\
& \left. + 4(m-1)^2 (\overline{m}+1)^2 m(m-1)(\overline{m}+1) \right. \\
& \left. + (I-m)(I+m+1)(J+\overline{m})(J-\overline{m}+1) \right. \\
& \left. + (I+m)(I-m+1)(J-\overline{m})(J+\overline{m}+1) \right. \\
& \left. + (I+m-1)(I-m+2)(J+\overline{m}+2)(J-\overline{m}) \right. \\
& \left. + \delta_{m',m+1} \delta_{\overline{m}',\overline{m}-1} \alpha_{m,+}^I \alpha_{\overline{m},-}^J \left[4m^2 \overline{m}^2 \right. \right. \\
& \left. + 4(m+1)^2 (\overline{m}-1)^2 + 4m\overline{m}(m-1)(\overline{m}+1) \right. \\
& \left. + (I+m)(I-m+1)(J-\overline{m})(J+\overline{m}+1) \right. \\
& \left. + (I-m)(I+m+1)(J+\overline{m})(J-\overline{m}+1) \right. \\
& \left. + (I+m+2)(I-m-1)(J+\overline{m}-1)(J-\overline{m}+2) \right] \\
& \left. + \frac{1}{4} \delta_{m',m+2} \delta_{\overline{m}',\overline{m}-2} \alpha_{m,+}^I \alpha_{m+1,+}^I \alpha_{\overline{m},-}^J \alpha_{\overline{m}-1,-}^J \times \right. \\
& \times [(m+2)(\overline{m}-2) + m\overline{m} + (m+1)(\overline{m}-1)] \\
& \left. + \frac{1}{4} \delta_{m',m-2} \delta_{\overline{m}',\overline{m}+2} \alpha_{m,-}^I \alpha_{m-1,-}^I \alpha_{\overline{m},+}^J \alpha_{\overline{m}+1,+}^J \times \right. \\
& \times [(m-2)(\overline{m}+2) + m\overline{m} + (m-1)(\overline{m}+1)] \\
& \left. + \frac{1}{8} \delta_{m',m+3} \delta_{\overline{m}',\overline{m}-3} \alpha_{m,+}^I \alpha_{m+1,+}^I \alpha_{m+2,+}^I \times \right. \\
& \times \alpha_{\overline{m},-}^J \alpha_{\overline{m}-1,-}^J \alpha_{\overline{m}-2,-}^J \\
& \left. + \frac{1}{8} \delta_{m',m-3} \delta_{\overline{m}',\overline{m}+3} \alpha_{m,-}^I \alpha_{m-1,-}^I \alpha_{m-2,-}^I \times \right. \\
& \times \alpha_{\overline{m},+}^J \alpha_{\overline{m}+1,+}^J \alpha_{\overline{m}+2,+}^J \left. \right\},
\end{aligned} \tag{124}$$

where in the simplest approximation in which the matrix elements do not depend upon n and L ,

$$\begin{aligned}
K_0 = & -\frac{1}{3} B(I, J) I(I+1) J(J+1) \\
& - 5C(I, J) I(I+1) J(J+1),
\end{aligned} \tag{125}$$

$$K_1 = A(I, J) + \frac{1}{2} B(I, J) + \frac{1}{5} C(I, J), \tag{126}$$

$$\begin{aligned}
K_2 = & B(I, J) + 2C(I, J) \left[-3I(I+1) J(J+1) \right. \\
& \left. + I(I+1) + J(J+1) + 3 \right],
\end{aligned} \tag{127}$$

$$K_3 = C(I, J), \tag{128}$$

where $A(I, J)$, $B(I, J)$, and $C(I, J)$ are given elsewhere [5]. Then, the equation for the energy eigenvalues for the magnetic dipole, electric quadrupole, and magnetic octupole interactions for arbitrary I, J is

$$\det(\hat{H}_0 + \hat{M} - E \mathbf{1}_n \otimes \mathbf{1}_e) = 0. \tag{129}$$

We note that some atoms can have couplings between different J values, and the K_i can often depend upon the other atomic quantum numbers such as n and L [6]. We have not considered such cases, but the K_i can be considered to have more general forms.

The simplest example that includes the electric quadrupole moment but not the magnetic octupole moment is for $I = 1$ and $J = 1/2$, as for the ground ${}^2S_{1/2}$ state of ${}^2\text{H}$ and the ${}^2\text{S}_{1/2}$ and ${}^2\text{P}_{1/2}$ excited states of ${}^{14}\text{N}$ [9]. The rank-6 matrix $\hat{H}_0 + \hat{M}$ has horizontal elements (m, \overline{m}) and vertical elements (m', \overline{m}') . One may define the upper left corner element to be $(m', \overline{m}') = (1, \frac{1}{2})$ and $(m, \overline{m}) = (1, \frac{1}{2})$, and from far left to far right, the (m, \overline{m}) elements to be $(1, \frac{1}{2}), (1, -\frac{1}{2}), (0, \frac{1}{2}), (0, -\frac{1}{2}), (-1, \frac{1}{2}),$ and $(-1, -\frac{1}{2})$. The same order applies from top to bottom for the (m', \overline{m}') states. Then the six diagonal elements of $\hat{H}_0 + \hat{M}$ from upper left corner to lower right corner are respectively $\hbar(\Omega_e/2 + \Omega_n) + K_0 + \frac{1}{2}K_1 + \frac{1}{4}K_2$, $-\hbar(\Omega_e/2 - \Omega_n) + K_0 - \frac{1}{2}K_1 + \frac{3}{4}K_2$, $\hbar\Omega_e/2 + K_0 + \frac{1}{2}K_2$, $-\hbar\Omega_e/2 + K_0 + \frac{1}{2}K_2$, $\hbar(\Omega_e/2 - \Omega_n) + K_0 - \frac{1}{2}K_1 + \frac{3}{4}K_2$, and $\hbar(\Omega_e/2 - \Omega_n) + K_0 + \frac{1}{2}K_1 + \frac{1}{4}K_2$. There are four non-vanishing off-diagonal elements. The second row $(m', \overline{m}') = (1, -\frac{1}{2})$ and third column $(m, \overline{m}) = (0, \frac{1}{2})$ element is

$$\Gamma \equiv \frac{1}{\sqrt{2}} \left(K_1 - \frac{K_2}{2} \right). \tag{130}$$

The third row $(m', \overline{m}') = (0, \frac{1}{2})$ and second column element $(m, \overline{m}) = (1, -\frac{1}{2})$ is also Γ . The fourth row $(m', \overline{m}') = (0, -\frac{1}{2})$ and fifth column $(m, \overline{m}) = (1, -\frac{1}{2})$ element is also Γ , and the fifth row $(m', \overline{m}') = (1, \frac{1}{2})$ and fourth column $(m, \overline{m}) = (0, -\frac{1}{2})$ element is also Γ .

Then, it is relatively easy to see that the determinant leads to two energy solutions linear in the K_i and the four solutions of two quadratic equations for E . The two

linear solutions for the energy in the nuclear moments are

$$E_1 = \hbar(\Omega_e/2 + \Omega_n) + K_0 + K_1/2 + K_2/4, \quad (131)$$

$$E_6 = -\hbar(\Omega_e/2 + \Omega_n) + K_0 + K_1/2 + K_2/4, \quad (132)$$

which correspond to the energies of the $(m, \bar{m}) = (1, \frac{1}{2})$ and $(-1, -\frac{1}{2})$ states, respectively. The four solutions of the two quadratic equations are

$$E_{2,4} = K_0 + \frac{1}{2} \left(\hbar\Omega_n + K_2 - \Gamma/\sqrt{2} \pm \sqrt{(\hbar\Omega_e - \hbar\Omega_n + \Gamma/\sqrt{2})^2 + 4\Gamma^2} \right), \quad (133)$$

$$E_{3,5} = K_0 + \frac{1}{2} \left(-\hbar\Omega_n + K_2 - \Gamma/\sqrt{2} \pm \sqrt{(\hbar\Omega_e - \hbar\Omega_n - \Gamma/\sqrt{2})^2 + 4\Gamma^2} \right), \quad (134)$$

so that all of the E_i are real. $E_{2,4}$ correspond respectively for small Γ to the $(m, \bar{m}) = (1, -\frac{1}{2})$ and $(0, \frac{1}{2})$ states, and $E_{3,5}$ correspond respectively for small Γ to the $(m, \bar{m}) = (0, -\frac{1}{2})$ and $(-1, \frac{1}{2})$ states.

For the $^4S_{\frac{3}{2}}$ ground state and $^2D_{\frac{3}{2}}$ excited state of ^{14}N [9], the K_2 contributions are generally stronger than for the $J = 1/2$ states solved above. The diagonal elements of \hat{M} for the two $(m, \bar{m}) = (\pm 1, \mp \frac{3}{2})$ states are $K_0 - \frac{3}{2}K_1 + \frac{15}{4}K_2$, those for the $(\pm 1, \mp \frac{1}{2})$ states are $K_0 - \frac{1}{2}K_1 + \frac{9}{4}K_2$, those of the $(\pm 1, \pm \frac{1}{2})$ states are $K_0 + \frac{1}{2}K_1 + \frac{7}{4}K_2$, those for the $(\pm 1, \pm \frac{3}{2})$ states are $K_0 + \frac{3}{2}K_1 + \frac{9}{4}K_2$, those for the $(0, \pm \frac{1}{2})$ states are $K_0 + \frac{7}{4}K_2$, and those for the $(0, \pm \frac{3}{2})$ states are $K_0 + \frac{3}{2}K_2$.

Of course, there are also considerably more nonvanishing off-diagonal elements of \hat{M} that contain K_2 than for the $^2S_{\frac{1}{2}}$ and $^2P_{\frac{1}{2}}$ states. The $^2D_{\frac{5}{2}}$ excited state of ^{14}N is even more complicated. For this electronic state, the diagonal elements for the two $(m, \bar{m}) = (\pm 1, \pm \frac{5}{2})$ states are $K_0 + \frac{5}{2}K_1 + \frac{25}{4}K_2$, those of the $(\pm 1, \pm \frac{3}{2})$ states are $K_0 + \frac{3}{2}K_1 + \frac{19}{4}K_2$, those for the $(\pm 1, \pm \frac{1}{2})$ states are $K_0 + \frac{1}{2}K_1 + \frac{17}{4}K_2$, those for the $(\pm 1, \mp \frac{1}{2})$ states are $K_0 - \frac{1}{2}K_1 + \frac{19}{4}K_2$, those for the $(\pm 1, \mp \frac{3}{2})$ states are $K_0 - \frac{3}{2}K_1 + \frac{25}{4}K_2$, those for the $(\pm 1, \mp \frac{5}{2})$ states are $K_0 - \frac{5}{2}K_1 + \frac{35}{4}K_2$, those for the $(0, \pm \frac{5}{2})$ states are $K_0 + \frac{5}{2}K_2$, those for the $(0, \pm \frac{3}{2})$ states are $K_0 + \frac{13}{2}K_2$, and those for the $(0, \pm \frac{1}{2})$ states are $K_0 + \frac{17}{2}K_2$. There are also many different off-diagonal matrix elements. The full solutions of the electric quadrupole moment for each of the states of ^{14}N with filled $1s$ and $2s$ electronic orbitals to first order in perturbation theory will be presented elsewhere.

Details of these first order results for specific atoms and additional higher order results for the electric quadrupole, magnetic octupole, and electric hexadecapole moment using this RWF magnetic field Hamiltonian as the actual experimental probe will be published

elsewhere [1]. More complicated time-dependent interactions involving $\delta\hat{V}_{n,i}(t) + \delta\hat{V}_{e,i}(t)$ cases can be treated in the interaction representation once the transformation to the doubly-rotated basis is made [15, 16, 24, 27]. Specific examples of all of these cases will be presented in future publications.

An atom of particular interest in ^7Li , which has $I = \frac{3}{2}$ and its ground electronic state is $^2S_{1/2}$. The two electronic excited states are $^2P_{1/2}$ and $^2P_{3/2}$. From Table I, there have been nine measurements of its electric quadrupole moment, and they do not all agree with one another. We suggest that the RWF magnetic field measurements could be useful to obtain more reliable results for the electric quadrupole and magnetic octupole moments for that atom. A computer program for those computations is available [23].

We remark that it is possible to also use the analogous extension of Gottfried's wave function $|\psi_{G,n}(t)\rangle$, given by Eq. (8), to include the same perturbation expansion that includes the nuclear moments. We could write the analogous electronic wave function as

$$|\psi_{G,e}(t)\rangle = e^{-i\omega t J_z/\hbar} e^{-i\hat{\mathbf{n}}_e \cdot \mathbf{J} \Omega_e t/\hbar} |\psi_{G,e}(0)\rangle, \quad (135)$$

$$\begin{aligned} |\psi_{G,ne}(t)\rangle &= |\psi_{G,n}(t)\rangle \otimes |\psi_{G,e}(t)\rangle \\ &= e^{-i\omega t (I_z \mathbf{1}_e + \mathbf{1}_n J_z)/\hbar} \\ &\quad \times e^{-it(\hat{\mathbf{n}}_n \cdot \mathbf{I} \Omega_n \mathbf{1}_e + \Omega_e \mathbf{1}_n \hat{\mathbf{n}}_e \cdot \mathbf{J})/\hbar} \\ &\quad \times |\psi_{G,ne}(0)\rangle, \end{aligned} \quad (136)$$

where

$$|\psi_{G,ne}(0)\rangle = |\psi_{G,n}(0)\rangle \otimes |\psi_{G,e}(0)\rangle, \quad (137)$$

$$\hat{\mathbf{n}}_e = \hat{\mathbf{z}} \cos(\beta_e) + \hat{\mathbf{x}} \sin(\beta_e), \quad (138)$$

and where $\sin(\beta_e)$ and $\cos(\beta_e)$ are given by Eq. (48) and Ω_e is given by Eq. (49). Then, letting

$$\begin{aligned} |\tilde{\psi}_{G,ne}(t)\rangle &= e^{i(\beta_n I_y \mathbf{1}_e + \beta_e \mathbf{1}_n) J_y/\hbar} e^{i\omega t (I_z \mathbf{1}_e + \mathbf{1}_n J_z)/\hbar} |\psi_{G,ne}(t)\rangle \\ &= e^{i(\beta_n I_y \mathbf{1}_e + \beta_e \mathbf{1}_n J_y)/\hbar} \\ &\quad \times e^{-it(\hat{\mathbf{n}}_n \cdot \mathbf{I} \Omega_n \mathbf{1}_e + \mathbf{1}_n \hat{\mathbf{n}}_e \cdot \mathbf{J} \Omega_e)/\hbar} \\ &\quad \times |\psi_{G,ne}(0)\rangle, \end{aligned} \quad (139)$$

and then

$$\begin{aligned} i\hbar \frac{\partial}{\partial t} |\tilde{\psi}_{G,ne}(t)\rangle &= e^{i(\beta_n I_y \mathbf{1}_e + \beta_e \mathbf{1}_n J_y)/\hbar} \\ &\quad \times (\hat{\mathbf{n}}_n \cdot \mathbf{I} \Omega_n \mathbf{1}_e + \mathbf{1}_n \hat{\mathbf{n}}_e \cdot \mathbf{J} \Omega_e) \\ &\quad \times e^{-it(\hat{\mathbf{n}}_n \cdot \mathbf{I} \Omega_n \mathbf{1}_e + \mathbf{1}_n \hat{\mathbf{n}}_e \cdot \mathbf{J} \Omega_e)/\hbar} |\psi_{G,ne}(0)\rangle \\ &= e^{i(\beta_n I_y + \beta_e J_y)/\hbar} \\ &\quad \times (\hat{\mathbf{n}}_n \cdot \mathbf{I} \Omega_n \mathbf{1}_e + \mathbf{1}_n \hat{\mathbf{n}}_e \cdot \mathbf{J} \Omega_e) \\ &\quad \times e^{-i(\beta_n I_y \mathbf{1}_e + \mathbf{1}_n \beta_e J_y)/\hbar} e^{i(\beta_n I_y \mathbf{1}_e + \mathbf{1}_n \beta_e J_y)/\hbar} \\ &\quad \times e^{-it(\hat{\mathbf{n}}_n \cdot \mathbf{I} \Omega_n \mathbf{1}_e + \mathbf{1}_n \hat{\mathbf{n}}_e \cdot \mathbf{J} \Omega_e)/\hbar} |\psi_{G,ne}(0)\rangle \\ &= (\Omega_n I_z \mathbf{1}_e + \Omega_e \mathbf{1}_n J_z) |\tilde{\psi}_{G,ne}(t)\rangle, \end{aligned} \quad (140)$$

after doing the rotations about the \mathbf{y} axis for both the nuclear and electronic components, as described for the former in Sec. II.

B. Time-dependent perturbations

The exact wave function for the RWA to the problems of NMR and EPR should be suitable for use as the starting point for future time-dependent perturbations, in order to more closely approximate the actual experimental situations. A time-dependent perturbation of particular interest is $\delta\hat{V}_1(t)$ given by Eq. (79).

For the simple case $a_p = 0$ for $p \geq 2$, this would allow for a well-defined method to perturbatively treat the Hamiltonian $\hat{H}(t) = \omega_{n0}I_z + \omega_{n1}I_x \cos(\omega t)$ [39] and its corresponding EPR equivalent, as in early experiments [12]. More general perturbations for a large class of periodic fields along \hat{x} can be treated for suitable a_p and initial time t_0 [57]. This could treat square-wave and kinky (or triangular-wave) perturbations of various shapes, for example.

This technique could also be useful for time-dependent perturbative treatments of current “magic-angle” spinning magnetic resonance experiments in biophysics and organic chemistry [58], for which the time-dependent perturbation $\delta\hat{V}_2(t)$ is given by Eq. (82). In such cases, the perturbation form can be obtained by initially starting with the strong field $\mathbf{H}_0 = H_0[\hat{x} \sin \theta_M + \hat{z} \cos \theta_M]$, and the sample rotating at some small angle α about the \mathbf{z} axis, so that the effective magnetic field from the sample rotation at the angular frequency ω is $\mathbf{H}_1(t) = H_1[\hat{x} \cos(\omega t) + \hat{y} \sin(\omega t)]$. Then, by rotating $\mathbf{H}_0 + \mathbf{H}_1(t)$ by θ_M about the \mathbf{y} axis, the effective Hamiltonian in the laboratory frame pictured in Fig. 1 of [58]. Using the doubly-rotated bare wave function given by Eq. (103), \hat{H}_0 is diagonal and independent of t , so that the time-dependent perturbations can be carried out in the interaction representation [15, 16, 27].

VII. SUMMARY AND CONCLUSIONS

Gottfried’s elegant solution for the wave function of the rotating wave approximation to the nuclear magnetic resonance problem for general spin I allows one to simply calculate the probability of a transition from a fully-occupied state to any other fully-occupied state [15]. But it does not allow one to calculate the probability of a transition from a fully general mixed state to another fully general mixed state. By diagonalizing Gottfried’s wave function, we found a more useful exact wave function that allows such full generality of state transitions. Since the time-dependent applied magnetic field in the rotating wave approximation also applies to the electrons in an atom or molecule, an equivalent version of our more useful nuclear wave function applicable to electron paramagnetic resonance for a general electronic

isotope	I	P	μ_n/μ_N	Q (b)	atomic %
^1H	1/2	+	+2.79284734(3)		99.985
^2H	1	+	+0.85743822(9)	+0.00285783(30)	0.0135
^7Li	3/2	-	+3.256427(2)	-0.0370(8) to +3.2564625(4)	92.41 0.059(8) (9 values)
^{13}C	1/2	-	+0.7024118(14)		1.1
^{14}N	1	+	+0.40376100(6)	+0.02044(3)	99.6
^{15}N	1/2	-	-0.28318884(5)		0.38
^{17}O	5/2	+	-1.89379(9)	-0.02558(22)	0.037
^{29}Si	1/2	+	-0.55529(3)		4.67
^{31}P	1/2	+	+1.13160(3)		100
^{33}S	3/2	+	+0.6438212(14)	-0.0694(4)	0.75
^{43}Ca	7/2	-	-1.3173(6)	-0.408(8)	0.135
^{57}Fe	1/2	-	+0.0906		2.119
^{87}Sr	9/2	+	-1.0936030(13)	+3.05(2)	7.00
^{133}Cs	7/2	+	+2.582025(3)	-0.00355(4)	100
				+2.5829128(15)	-0.00371(4)

TABLE I. Table of the stable isotopes, spin quantum numbers I , parity P , nuclear magnetic moments μ_n relative to the nuclear magneton $\mu_N = (e\hbar)/(2m_p) = 5.05783699(31) \times 10^{-27}$ J/T, the electric quadrupole moment Q in barns (1 b = 10^{-28} m 2), and atomic % abundances, of the atoms in adenine, cytosine, guanine, and thymine, three isotopes of possible chemical defect substitutions, Si, P and S, respectively for C, N and O, and three isotopes present in blood and bones. ^7Li and ^{133}Cs are also listed.[1, 2, 50] More recent and complete tables of the alkali are available [6].

total angular momentum operator J was found. With both more useful wave function components, we showed that a wave function form that is rotated about both the nuclear and electronic variables by the appropriate but greatly different nuclear and electronic rotation angles leads to a bare time-independent Hamiltonian \hat{H}_0 that is diagonal in both the nuclear and electronic variables. This \hat{H}_0 allows for the calculation of the nuclear moment interactions proportional to sums of powers of $\mathbf{I} \cdot \mathbf{J}$ using standard time-independent perturbation theory. The elements of the matrix for the energies due to the magnetic dipole and electric quadrupole moment in an RWA experiment are found for general I, J . Exact expressions for the energies of the simplest case of $I = 1$ and $J = \frac{1}{2}$, corresponding to the $^2\text{P}_{\frac{1}{2}}$ and $^2\text{S}_{\frac{1}{2}}$ excited states of ^{14}N are presented. In addition, this simple form of \hat{H}_0 allows for treatments of time-dependent perturbations in the standard interaction representation.

We propose a new experimental technique to measure the nuclear moments of atoms and molecules. One can construct the applied magnetic field to have a strong constant component in one direction and a weaker circularly-rotating component normal to it. One would like to be able to vary the frequencies within at least an order of magnitude of both the nuclear magnetic resonance and the electron paramagnetic resonance frequencies, which differ by several orders of magnitude. This may require two separate devices.

This work also applies to molecules with sufficiently high symmetry that the molecular total angular momen-

tum in the absence of the applied field is quantized in terms of a set of J values. In molecules with high symmetry, such as benzene, this should be possible. But in steric molecules such as a C atom bonded to four different atomic or molecular groups, such as H, Cl, NH₂, and OH, there is no center of symmetry, and hence no set of single J values. The relevant point is that for molecules without high symmetry, such as each of the four amino acids in DNA, there is a mirror plane through the flat molecule, but none of these molecules exhibits rotational symmetry about the axis normal to that plane. Thus, it is possible that mixed angular momentum states J_1 and J_2 could be present in them. But how do we characterize the mixing parameter and its phase? Those are questions for future investigations.

VIII. APPENDIX

Gottfried used the notations $\hbar = 1$, \mathbf{J} for our \mathbf{I} , Ω for our ω_0 , $\lambda\Omega$ for our ω_1 , Δ for our Ω , φ for our β , and his $\hat{H}_{RWA}(t)$ was opposite in sign to ours [15]. Although Gottfried was the first to correctly diagonalize $\hat{H}_{RWA}(t)$, he wrote the wave function $|\psi(t)\rangle \equiv |t\rangle$ in our notation as

$$|\psi(t)\rangle = e^{-iI_z\omega t/\hbar} e^{-i\hat{\mathbf{n}} \cdot \mathbf{I} \Omega t/\hbar} |\psi(0)\rangle, \quad (141)$$

$$\hat{\mathbf{n}} = \hat{\mathbf{z}} \cos \beta + \hat{\mathbf{x}} \sin \beta, \quad (142)$$

where $\hat{\mathbf{z}} = \hat{\mathbf{u}}_z$, $\hat{\mathbf{x}} = \hat{\mathbf{u}}_x$.

In order to clarify the equality of the matrix elements of Gottfried's wave function, Eq. (8), and the present wave function, Eq. (35), we shall demonstrate their equivalence for $I = 1$. In this case, it is easy to show that for $I = 1$, $\langle I, m' | (\mathbf{I} \cdot \hat{\mathbf{n}}/\hbar)^3 | I, m \rangle = \langle I, m' | \mathbf{I} \cdot \hat{\mathbf{n}}/\hbar | I, m \rangle$. Letting $\zeta = \Omega t$ and $\hat{Q} = [I_z \cos(\beta) + I_x \sin(\beta)]/\hbar = \mathbf{I} \cdot \hat{\mathbf{n}}/\hbar$, where $\hat{\mathbf{n}} = \hat{\mathbf{z}} \cos(\beta) + \hat{\mathbf{x}} \sin(\beta)$ and $\sin(\beta)$ and $\cos(\beta)$ are given in Eq. (10). Then letting $|I, m\rangle \equiv |m\rangle$ for $I = 1$,

$$\begin{aligned} d_{m',m}^{(1)}(\beta, \zeta) &\equiv \langle m' | e^{-i\zeta \hat{Q}} | m \rangle \\ &= \langle m' | \mathbf{1} - i \sin(\zeta) \hat{Q} - [1 - \cos(\zeta)] \hat{Q}^2 | m \rangle \end{aligned} \quad (143)$$

where the matrix elements satisfy

$$\begin{aligned} d_{1,1}^{(1)} &= -i \sin(\zeta) \cos(\beta) + \frac{1}{2} (\sin^2(\beta) + \cos(\zeta)[1 + \cos^2(\beta)]) \\ &= d_{-1,-1}^{(1)*}, \end{aligned}$$

$$d_{0,0}^{(1)} = \cos^2(\beta) + \sin^2(\beta) \cos(\zeta),$$

$$\begin{aligned} d_{1,0}^{(1)} &= d_{0,1}^{(1)} = -\frac{\sin(2\beta)}{2\sqrt{2}} [1 - \cos(\zeta)] \\ &\quad - \frac{i}{\sqrt{2}} \sin(\beta) \sin(\zeta), \end{aligned}$$

$$d_{1,-1}^{(1)} = d_{-1,1}^{(1)} = -\frac{1}{2} \sin^2(\beta) [1 - \cos(\zeta)],$$

$$d_{0,-1}^{(1)} = d_{-1,0}^{(1)} = -d_{1,0}^{(1)*}.$$

It can also be shown that for general I ,

$$\langle m' | e^{-i\beta I_y/\hbar} e^{-i\zeta I_z/\hbar} e^{i\beta I_y/\hbar} | m \rangle = d_{m',m}^{(I)}(\beta, \zeta). \quad (149)$$

For $I = 1$, each component of $d_{m',m}^{(1)}(\beta, \zeta)$ is identical to that calculated above. However, this expression can readily be evaluated for arbitrary I , and one does not require the individual matrix evaluations for each I value, as outlined above for $I = 1$.

Gottfried did this for $I = \frac{1}{2}$ using the Pauli matrices [15]. He showed that the matrix elements could be written as

$$\begin{aligned} D_{\hat{\mathbf{n}}}(\Omega t) &= e^{-i(\hat{\mathbf{n}} \cdot \boldsymbol{\sigma})\Omega t/2} \\ &= \mathbf{1} \cos(\Omega t/2) - i \hat{\mathbf{n}} \cdot \boldsymbol{\sigma} \sin(\Omega t/2) \end{aligned} \quad (150)$$

in our notation. Since the standard rotation matrix involves time-independent rotations by the angle β about the $\hat{\mathbf{y}}$ axis, for $I = \frac{1}{2}$, $d_{m',m}^{(1/2)}(\beta)$ has diagonal matrix elements $\cos(\beta/2)$ and off-diagonal matrix elements $\mp \sin(\beta/2)$. Then, he wrote that the probability of a transition from state m to state m' , either for diagonal or off-diagonal states, would be $|d_{m',m}^{(1/2)}(\beta)|^2$ with β given by $\sin(\beta/2) = \frac{\omega_1}{\Omega} \sin(\Omega t/2)$ [15].

But he also wrote that this would apply for the general $d_{m',m}^{(I)}(\beta)$ with β also given by $\sin(\beta/2) = \frac{\omega_1}{\Omega} \sin(\Omega t/2)$. This statement may have confused some workers in NMR. What he should have written was that the expression for the general diagonal or off-diagonal (m', m) states for general $d_{m',m}^{(I)}(\beta)$ could be equated with the appropriate elements of that time-dependent matrix. Thus, for $I = 1$, $d_{m',m}^{(1)}(\beta)$ has the off-diagonal elements

$$d_{1,0}^{(1)} = d_{0,-1}^{(1)} = -d_{0,1}^{(1)} = -d_{-1,0}^{(1)} = -\frac{1}{\sqrt{2}} \sin(\beta) \quad (144)$$

and $d_{1,-1}^{(1)} = d_{-1,1}^{(1)} = \frac{1}{2} [1 - \cos(\beta)]$ [16]. For each of these off-diagonal matrix elements, these $|d_{m',m}^{(1)}(\beta)|^2$ values are

consistent with the $|d_{m',m}^{(1)}(\beta = \sin^{-1}(\omega_1/\Omega), \zeta = \Omega t)|^2$ presented in Eqs. (146) to (148). We have shown analytically for the diagonal matrix elements $d_{0,0}^{(1)} = \cos(\beta)$

and $d_{1,1}^{(1)} = d_{-1,-1}^{(1)*} = \frac{1}{2} [1 + \cos(\beta)]$ that this consistency applies to every matrix element. We also found numerically that it is true for every (m', m) combination, both

diagonal and off-diagonal, of every spin $\frac{3}{2}$ combination of

$$(147) |d_{m',m}^{(\frac{3}{2})}(\beta)|^2.$$

(148) The transformed time-dependent perturbations are

listed in the following. We have for the nuclear cases,

$$\begin{aligned}\widetilde{\delta\hat{V}}_{n1}(t) = & -\omega_{n1} \sin(\omega t) \left[I_y \cos(\omega t) \right. \\ & + \sin(\omega t) \left(I_x \cos(\beta_n) + I_z \sin(\beta_n) \right) \\ & \left. + \omega_{n1} \left[\cos(\omega t) \left(I_x \cos(\beta_n) + I_z \sin(\beta_n) \right) \right. \right. \\ & \left. \left. - I_y \sin(\omega t) \right] \sum_{p=2}^{\infty} a_p \cos[p\omega(t-t_0)] \right], \quad (151)\end{aligned}$$

$$\begin{aligned}\widetilde{\delta\hat{V}}_{n2}(t) = & 2\omega_{n1} \sin\theta \cos(\omega t) \\ & \times \left[I_z \left(\cos\theta \cos(\beta_n) - \sin\theta \sin(\beta_n) \cos(\omega t) \right) \right. \\ & \left. - I_x \left(\cos\theta \sin(\beta_n) + \sin\theta \cos(\beta_n) \cos(\omega t) \right) \right. \\ & \left. - I_y \sin\theta \sin(\omega t) \right]. \quad (152)\end{aligned}$$

For the electronic cases,

$$\begin{aligned}\widetilde{\delta\hat{V}}_{e1}(t) = & -\omega_{e1} \sin(\omega t) \left[J_y \cos(\omega t) \right. \\ & + \sin(\omega t) \left(J_x \cos(\beta_e) + J_z \sin(\beta_e) \right) \left. \right] \\ & + \omega_{e1} \left[\cos(\omega t) \left(J_x \cos(\beta_e) + J_z \sin(\beta_e) \right) \right. \\ & \left. - J_y \sin(\omega t) \right] \sum_{p=2}^{\infty} a_p \cos[p\omega(t-t_0)], \quad (153)\end{aligned}$$

$$\begin{aligned}\widetilde{\delta\hat{V}}_{e2}(t) = & 2\omega_{e1} \sin\theta \cos(\omega t) \\ & \times \left[J_z \left(\cos\theta \cos(\beta_e) - \sin\theta \sin(\beta_e) \cos(\omega t) \right) \right. \\ & \left. - J_x \left(\cos\theta \sin(\beta_e) + \sin\theta \cos(\beta_e) \cos(\omega t) \right) \right. \\ & \left. - J_y \sin\theta \sin(\omega t) \right]. \quad (154)\end{aligned}$$

IX. ACKNOWLEDGMENTS

The authors acknowledge discussions with Luca Argenti, Bo Chen, James K. Harper, and Talat S. Rahman. R. A. K. was partially supported by the U. S. Air Force Office of Scientific Research (AFOSR) LRIR #24RQCOR004, and the AFRL/SFFP Summer Faculty Program provided by AFRL/RQ at WPAFB.

[1] N. J. Stone, Table of nuclear dipole and electric quadrupole moments, *Atomic Data and Nuclear Data Tables* **90**, 75-176 (2005)

[2] Commission on Isotopic Abundances and Atomic Weights (CIAAW), ciaaw.org, International Union of Pure and Applied Chemistry (IUPAC), and the University of Alberta, Canada, Chemistry Department table of atomic mass abundances, https://www.chem.ualberta.ca/~massspec/atomic_mass_abund.pdf

[3] N. R. Ramsey, *Nuclear Moments*, (John Wiley & Sons, New York, 1953).

[4] R. E. Trees, Hyperfine structure formulas for LS coupling, *Phys. Rev.* **92**, (2), 308-314 (1953).

[5] L. Armstrong, Jr., *Theory of the Hyperfine Structure of Free Atoms*, (Wiley-Interscience, New York, 1971).

[6] M. Allegrini, E. Arimando, and L. A. Orozco, Survey of alkali structure measurements in alkali atoms, *J. Phys. and Chem. Ref. Data* **51**, (4), 043102 (2022). <https://doi.org/10.1063/5.0098061>

[7] H. F. Schaefer III, R. A. Klemm, and F. E. Harris, Atomic hyperfine structure. I. Polarization wavefunctions for the ground states of B, C, N, O, and F, *Phys. Rev.* **176**, 49-58 (1968).

[8] H. F. Schaefer III, R. A. Klemm, and F. E. Harris, Atomic hyperfine structure. II. First-order wavefunctions for the ground states of B, C, N, O, and F, *Phys. Rev.* **181**, 137-143 (1969).

[9] H. F. Schaefer III and R. A. Klemm, Atomic hyperfine structure. III. Excited states of C, N, and O, *Phys. Rev.* **188**, 152-160 (1969). We note that the $^2S_{\frac{1}{2}}$ state of N was not calculated.

[10] E. Majorana, Atomi orientati in campo magnetico variabile, *Nuovo Cimento* **9**, 43-50 (1932).

[11] J. Schwinger, On angular momentum, Nuclear Development Associates (1952).

[12] I. I. Rabi, N. F. Ramsey, and J. Schwinger, Use of rotating coordinates in magnetic resonance problems, *Rev. Mod. Phys.* **26**, 167-171 (1954).

[13] N. R. Ramsey, *Molecular Beams*, (Clarendon Press, Oxford, UK 1956), App. E pp 427-430.

[14] J. Schwinger, The Majorana formula, *Trans. New York Acad. Sci.* pp 170-184 (1977).

[15] K. Gottfried, *Quantum Mechanics Vol. I: Fundamentals*, (W. A. Benjamin, Inc., New York, NY 1966).

[16] J. J. Sakurai and J. Napolitano, *Modern Quantum Mechanics*, (3rd Ed., Cambridge University Press, Cambridge, UK, 2021).

[17] L. H. Klemm, C. E. Klopfenstein, R. Zell, D. R. McCoy, and R. A. Klemm, Chemistry of thienopyridines. III. Synthesis of thieno[2,3-b]- and thieno[3,2-b]pyridine systems. Direct substitution into the former system, *J. Org. Chem.* **34**, (2), 347-354 (1969).

[18] L. H. Klemm, R. Zell, I. T. Barnish, R. A. Klemm, C. E. Klopfenstein, and D. R. McCoy, Chemistry of thienopyridines. IX. Direct nitration of thieno[2,3-b]pyridine and thieno[3,2-b]pyridine, *J. Heterocyclic Chem.* **7**, (2), 373-

379 (1970).

[19] L. H. Klemm, R. A. Klemm, P. S. Santhanum, and D. V. White, Intramolecular Diels-Alder reactions VI. Synthesis of 3-hydroxymethyl-2-naphthoic acid lactones, *J. Org. Chem.* **36**, 2169-2172 (1971).

[20] A. Bonfiglioli and R. Fulci, Topics in noncommutative algebra: The theorem of Campbell, Baker, Hausdorff, and Dynkin, in J.-M. Morel and B. Tessier, eds., *Springer Lecture Notes on Mathematics 2034* (Springer-Verlag, Berlin, Heidelberg, 2012), pp 125-126.

[21] Z. Liu, S. Kim, and R. A. Klemm, Nuclear magnetic resonance for arbitrary spin values in the rotating wave approximation, arXiv:2203.08755 [quant-ph] (2022). <https://doi.org/10.48550/arXiv.2203.08755>

[22] S. Kim, Doubly Rotating Coordinates: Wave functions in Magnetic Resonance Problems, Graduate Thesis and Dissertation 2023-2024. 130. <https://stars.library.ucf.edu/etd2023/130>.

[23] Z. Liu, Advancements in Nuclear Magnetic Resonance, Electron Paramagnetic Resonance, Multipole Moments, and Lie Group Properties, Graduate Thesis and Dissertation 2023-2024. 155. <https://stars.library.ucf.edu/etd2023/155>.

[24] D. J. Griffiths and D. J. Schroeter, *Introduction to Quantum Mechanics*, 3rd Ed., (Cambridge University Press, Cambridge, UK, 2018).

[25] M. Brink and G. R. Satchler, *Angular Momentum*, 3rd Ed. (Oxford University Press, Oxford, UK 1993).

[26] J. W. Rohlfs, *Modern Physics from α to Z^0* , (Wiley, New York, 1994).

[27] K. Gottfried and T.-M. Yan, *Quantum Mechanics: Fundamentals*, (2nd Ed., Springer Science + Business Media New York, NY 2003).

[28] B. E. Hall and R. A. Klemm, Microscopic model of the Knight shift in anisotropic and correlated metals, *J. Phys.: Condens. Matter* **28**, 03LT01 (2016).

[29] R. A. Klemm, Theory of the Knight shift in an anisotropic, multiband Type-II superconductor, *Magnetochemistry* **2018**, 4, 14. doi.org://10.3390/magnetochemistry4010014.

[30] C. Aragone, E. Chalbaud, and S. Salamó, On intelligent spin states, *J. Math. Phys.* **17**, 1963-1971 (1976).

[31] M. A. Rashid, The intelligent states. I. Group-theoretic study and the computation of matrix elements, *J. Math. Phys.* **19**, 1391-1296 (1978).

[32] J. H. Eberle, B. W. Shore, Z. Bialynicki-Birula, and I. Bialynicki-Birula, Coherent dynamics of N -level atoms and molecules I. Numerical experiments, *Phys. Rev. A* **16** (15), 2038-2047 (1977).

[33] Z. Bialynicki-Birula, I. Bialynicki-Birula, J. H. Eberle, and B. W. Shore, Coherent dynamics of N -level atoms and molecules I. Analytic solutions, *Phys. Rev. A* **16** (15), 2048-2054 (1977).

[34] R. J. Cook and B. W. Shore, Coherent dynamics of N -level atoms and molecules. III. An analytically soluble periodic case, *Phys. Rev. A* **20**,(2), 539-544 (1979).

[35] B. W. Shore and R. J. Cook, Coherent dynamics of N -level atoms and molecules. IV. Two- and three-level behavior, *Phys. Rev. A* **20** (5), 1958-1964 (1979).

[36] A. Amirav, U. Even, J. Jortner, and L. Kleinman, Coherent dynamics of multilevel systems, *J. Chem. Phys.* **73**, (9), 4217-4232 (1980).

[37] K. B. Whaley and J. C. Light, Rotating wave transformations: A new approximation for multiphoton absorption and dissociation in laser fields, *Phys. Rev. A* **29**, (3), 1188-1207 (1984).

[38] Y. Prior and A. N. Weiszmann, Quantum-theoretical description of coherent four-wave mixing, *Phys. Rev. A* **29**, (5), 2700-2707 (1984).

[39] E. Layton, Y. Huang, and S.-I. Chu, Cyclic quantum evolution and Aharonov-Anandan geometric phases in SU(2) spin-coherent states, *Phys. Rev. A* **41**, (1), 42-48 (1990).

[40] A. Amirav, U. Even, and J. Jortner, The dynamics of equally spaced multilevel model systems, *Int. J. Quant. Chem. vol. XXXIX*, 387-397, (1991).

[41] E. K. Irish, Generalized rotating-wave approximation for arbitrarily large coupling, *Phys. Rev. Lett.* **99**, 173401 (2007).

[42] F. T. Hioe, N-level quantum systems with SU(2) dynamic symmetry, *J. Opt. Soc. Am. B* **4**, 1327-1332 (1987).

[43] J. Petrovic, I. Herrera, P. Lombardi, F. Schäfer, and F. S. Cataliotti, A multi-state interferometer on an atom chip, *New J. Phys.* **15** 043002 (2013).

[44] T. Zanon-Willette, D. Wilkowski, R. Lefevre, A. V. Taichenachev, and V. I. Yudin, SU(2) hyper-clocks: Quantum engineering of spinor interferences for time and frequency metrology, *Phys. Rev. Research* **4**, 023117 (2022).

[45] F. Heiße, F. Köhler-Langes, S. Rau, J. Hau, S. Junek, A. Kracke, A. Mooser, W. Quint, S. Ulmer, G. Werth, K. Blauer, and S. Sturm, High-precision measurement of the proton's atomic mass, *Phys. Rev. Lett.* **119**, 033001 (2017).

[46] J. Schwinger, On quantum-electrodynamics and the magnetic moment of the electron, *Phys. Rev.* **73**, 416 (1948).

[47] T. Aoyama, T. Kinoshita, and M. Nio, Theory of the anomalous magnetic moment of the electron, *Atoms* **2019**, 7, 28.

[48] P. J. Mohr, D. B. Newell, and B. N. Taylor, CODATA recommended values of the fundamental constants: 2014, *Rev. Mod. Phys.* **88**, 035009 (2016).

[49] M. V. Berry, Quantal phase factors accompanying adiabatic changes, *Proc. Roy. Soc. Lond. A* **392**, 45-57 (1984).

[50] P. Pyykkö, Year-2017 nuclear quadrupole moments, *Mol. Phys.* **116**, 1328-1338 (2018).

[51] Institute of Chemistry, Hebrew University of Jerusalem, Jerusalem, Israel. Website for ^{14}N and ^{15}N NMR: <http://chem.ch.huji.ac.il/nmr/techniques/1d/row2/n.html>

[52] H.-L. Deng, X.-S. Luo, Z. Lin, J. Niu, and M.-H. Huang, ^{14}N NMR as a general tool to characterize the nitrogen-containing species and monitor the nitration process, *J. Org. Chem.* **86**, 16699-16706 (2021).

[53] S. Cavadini, A. Lupulesco, S. Antonijevic, and G. Bodenhausen, Nitrogen-14 NMR spectroscopy using residual dipolar splittings in solids, *J. Am. Chem. Soc.* **128**, 7706-7707 (2006).

[54] S. L. Veinberg, Z. W. Friedl, A. W. Lindquist, B. Kispal, K. J. Harris, L. A. O'Dell, and R. W. Schurko, ^{14}N Solid-state NMR spectroscopy of amino acids, *ChemPhysChem* **17**, 4011-4027 (2016).

[55] O. E. O. Zeman and T. Bräuniger, Quantifying the quadrupolar interaction by ^{45}Sc -NMR spectroscopy of single crystals, *Sol. State Nucl. Magn. Res.* **117**, 101775 (2022).

[56] J. T. Urban, Nuclear magnetic resonance studies of quadrupolar nuclei and dipolar field effects, Ph. D. thesis, University of California at Berkeley, Berkeley, CA, USA (2004)

[57] M. L. Boas, *Mathematical Methods in the Physical Sciences*, 3rd Ed., (Wiley, NY, USA, 2006).

[58] B. Reif, S. E. Ashbrook, L. Emsley, and M. Hong, Solid state NMR spectroscopy, *Nat. Rev. Methods Primers* **1**, 2 (2021). doi.org://10.1038/s43586-020-0002-1.

[59] D. Budker, D. R. Kimball, S. M. Rochester, and J. T. Urban, Alignment-to-orientation conversion and nuclear quadrupole resonance, *Chem. Phys. Lett.* **378**, 440-448 (2003).

[60] J. Schaefer and E. O. Stejskal, Carbon-13 nuclear magnetic resonance of polymers spinning at the magic angle, *J. Am. Chem. Soc.* **98**, 4, 1031-1032 (1976).

[61] L. Frydman and J. S. Harwood, Isotropic spectra of half-integer quadrupolar spins from bidimensional magic-angle spinning NMR, *J. Am. Chem. Soc.* **117**, 5367-5368 (1995).

[62] V. Gerginov, A. Derevianko, and C. Tanner, Observation of the nuclear magnetic octupole moment of ¹³³Cs, *Phys. Rev. Lett.* **91**, 072501 (2003).

[63] K. Beloy, A. Derevianko, and W. R. Johnson, Hyperfine structure of the metastable ³P₂ state of alkaline-earth-metal atoms as an accurate probe of nuclear magnetic octupole moments, *Phys. Rev. A* **77**, 052503 (2008).

[64] K. Beloy, A. Derevianko, V. A. Dzuba, G. T. Howell, B. B. Blinov, and E. N. Fortson, Nuclear magnetic octupole moment and the hyperfine structure of the 5D_{3/2,5/2} states of the Ba⁺ ion, *Phys. Rev. A* **77**, 052503 (2008).

[65] I. L. Moudrakovski, Recent advances in solid-state NMR of alkaline earth elements, *Annu. Rep. NMR Spectrosc.* **79**, 129-240 (2013).

[66] A. K. Singh, D. Angom, and V. Natarjan, Observation of the nuclear magnetic octupole moment of ¹⁷³Vb from precise measurements of the hyperfine structure in the ³P₂ state, *Phys. Rev. A* **87**, 012512 (2013).

[67] S. E. Ashbrook, S. Sneddon, New methods and applications in solid-state NMR spectroscopy of quadrupolar nuclei, *J. Am. Chem. Soc.* **136**, 15440-15446 (2014).

[68] C. Leroy and D. L. Bryce, Recent advances in solid-state nuclear magnetic resonance spectroscopy of exotic nuclei, *Prog. Nucl. Magn. Reson. Spectrosc.* **109**, 160-199 (2018).

[69] D. Xiao, J. G. Li, W. C. Campbell, T. Dellaert, P. McMillan, A. Ransford, C. Roman, and A. Derevianko, Hyperfine structure of ¹⁷³Yb⁺: Toward resolving the ¹⁷³Yb nuclear-octupole-moment puzzle, *Phys. Rev. A* **102**, 022810 (2020).

[70] R. de Groote, S. Kujanpää, Á. Koszorús, J. Li, and I. Moore, Magnetic octupole moment of ¹⁷³Yb using collinear laser spectroscopy, *Phys. Rev. A* **103**, 032826 (2021).

[71] M. E. Smith, Recent progress in solid-state nuclear magnetic resonance of half-integer spin low- γ quadrupolar nuclei applied to inorganic materials, *Magn. Reson. Chem.* **59**, 864-907 (2021).

[72] R. P. de Groote, J. Moreno, J. Dobaczewski, Á. Koszorús, I. Moore, M. Reponeu, B. K. Sahoo, and C. Yuan, Precision measurement of the magnetic octupole moment in ⁴⁵Sc as a test for state-of-the-art atomic- and nuclear-structure theory, *Phys. Lett. B* **827**, 136930 (2022).

[73] J. Li, G. Gaigalas, J. Bierón, J. Ekman, P. Jönsson, M. Godefroid, and C. Froese Fischer, Re-evaluation of the nuclear magnetic octupole moment of ²⁰⁹Bi, *Atoms* **2022**, 10, 132.

[74] B. Rahaman, S. C. Wright, and S. Dutta, Observation of quantum interference of optical transition pathways in Doppler-free two-photon spectroscopy for precision measurements, *Phys. Rev. A* **109**, 042820 (2024).

[75] J. R. Persson, Table of hyperfine anomaly in atomic systems-2023, *Atomic Data and Nuclear Data Tables* **154**, 101589 (2023).

[76] See Supplementary Material for additional figures for $\frac{5}{2} \leq I, J \leq \frac{9}{2}$.